European Journal of Navigation

Vol. 22 No 1.

The leading journal for systems, services and applications

April 2022

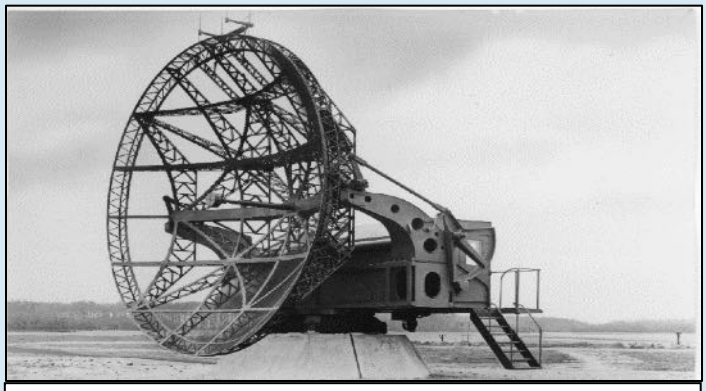

The Development of Radar Technology in Germany against the Background of Innovation Systems of Combatant Nations during World War II

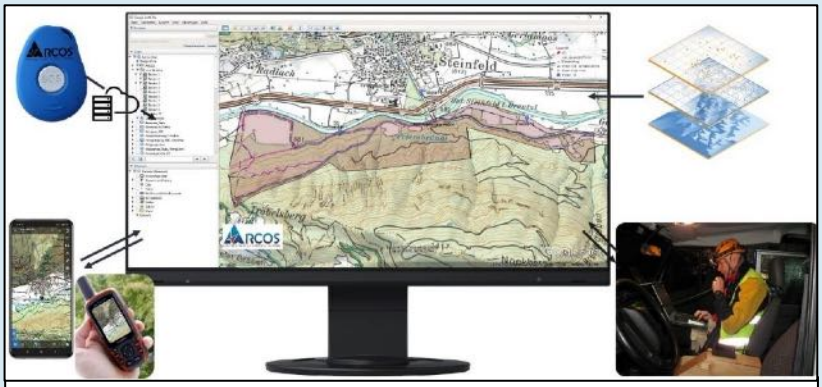

A Freely Usable Mission Control System for Mountain Rescue Operations based on Satellite Navigation, Live Tracking and Geoinformation Data

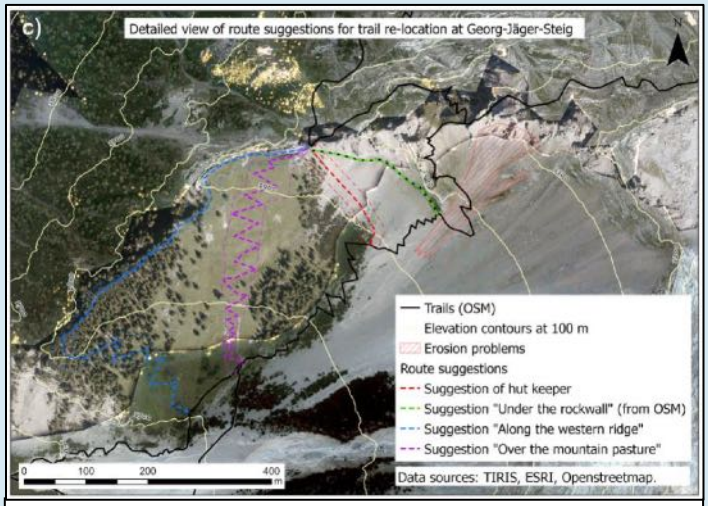

Earth Observation-based Assessment of Mass Movement Impact on Alpine Infrastructure Management

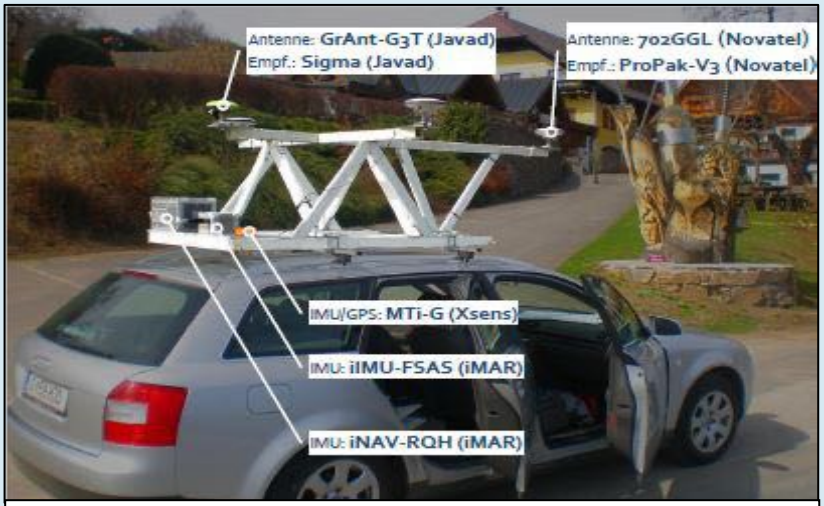

Tightly Coupled GPS/IMU Data Integration for the Estimation of Vehicle Trajectories

European Journal of Navigation
The leading journal for systems, services and applications

The European Journal of Navigation (EJN) is the common publication of presently five European Navigation Institutes (DGON, ION-CH, NIN, NNF, OVN) for its members and individual subscribers. The EJN is produced by BCMartens GbR, Germany.

Websites Contributing Institutes

DGON	www.dgon.de
ION-CH	www.ion-ch.ch
NIN	www.navnin.nl
NNF	www.nornav.org
OVN	www.ovn.at

© Copyright Cover Photos: Authors

ISSN not assigned
(only for print and online versions)

Editorial Contributions

All material submitted to the Producer and relating to EJN will be treated as unconditionally assigned for publication under copyright subject to the Producer's unrestricted right to edit and offer editorial comments.
BCMartens GbR assumes no responsibility for unsolicited material or for the accuracy of information thus received.

No material may be reproduced in whole or in part without written permission of BCMartens GbR.

Producer's Editorial

Dear readers,

with the following pages, we present the first EJN edition of 2022.

Look forward to very interesting articles from Austria (3) and Germany (1), covering the areas of

- Radar
- Mountain Rescue
- Alpine Infrastructure Management and
- Vehicle Trajectories

applications.
Enjoy reading!

Kind regards,

Bernd Martens

Please send your contributions to

EJN-Martens@magenta.de

The Development of Radar Technology in Germany Against the Background of Innovation Systems of Combatant Nations during World War II

Wolfgang Holpp, Helmut Klausing

The Roots of Radar Technology in Germany and Great Britain

It was in the year 1904 when Christian Hülsmeyer, a German engineer, filed the first radar patent of the world. However, nobody knew the word „radar“ at that time, it came into use about 30 years later, only [1], [2], [3].

On May 18, 1904, Hülsmeyer, just 22 years of age, gave a remarkable presentation of an apparatus he had constructed and built and which he called “Telemobiloskop”. In front of representatives of shipping companies and reporters from local newspapers, a very impressive public demonstration took place at the Dombrücke (today Hohenzollern Bridge) across the river Rhine in Cologne. The Telemobiloskop and its antennas were pointed towards the river and reliably rang a bell whenever a ship passed by. It must be clearly emphasized that this set-up was built without any amplifying elements like tubes or transistors; none of these devices being available in those days.


KAISERLICHES PATENTAMT

PATENTSCHRIFT

№ 165546

KLASSE 74c.

CHR. HÜLSMEYER IN DÜSSELDORF.

Verfahren, um entfernte metallische Gegenstände mittels elektrischer Wellen einem Beobachter zu melden.

Patentiert im Deutschen Reiche vom 30. April 1904 ab.

Fig. 1.

[2]

Figure 1: Christian Hülsmeyer in 1904 and his patent

By April 30, 1904, Hülsmeyer had already filed his invention at the German Patent Office in Berlin with the title „Verfahren, um entfernte metallische Gegenstände mittels elektrischer Wellen einem Beobachter zu melden“. The subsequent English patent of June 10, 1904, reads „Hertzian-wave Projecting and Receiving Apparatus Adapted to Indicate or Give Warning of the Presence of a Metallic Body, such as a Ship or a Train, in the Line of Projection of such Waves“.

Hülsmeyer's apparatus consisted of a transmit and receive antenna, a double spark gap radio frequency generator and a coherer as the receiving element. The operating frequency can only be presumed today, but based on the transmitter principle, a spectrum of several hundred Megahertz must have been emitted. The complete front-end could be rotated by 360° in azimuth synchronously with an electro-mechanical device which Hülsmeyer called "Kompass". This part of the Telemobiloskop indicated the direction of a target reflecting the incident waves.

The tragedy of Hülsmeyer's entire work on wireless direction finding was that in the end, he was unable to convince potential military or civil users and customers to provide long-term support for his invention. As well as this lack of interest on the part of his contemporaries, he also suffered from the fact that electronic techniques were still in their absolute infancy in the early 20th century. His ideas were, like those of many other inventors in history, far ahead of his times.

During the first quarter of the 20th century, wireless communication became the predominant application of electromagnetic waves. Hülsmeyer's invention had faded from memory. By 1895, the Italian Guglielmo Marconi added an antenna to a spark gap and transmitted telegraphic signals over several kilometres. His experimental achievements reached their zenith in 1901 when he bridged the Atlantic from England to Newfoundland with wireless signals; a distance of over 3,600 km [4], [5]. In the following years, aided by the parallel development of electronic techniques, Marconi's inventions spread to a wide commercial field. In 1922 he again recognized the possibility of detecting metallic objects by reflected electromagnetic radiation. And again his initiative, too, did not find any echo from the scientific and technical community.

Radar Technology's First Steps to Maturity

Marconi's ideas were taken up in the same year 1922 by two Americans, A. H. Taylor and L. C. Young from the US Naval Research Laboratory (NRL) who, while experimenting with frequencies of approximately 60 MHz, observed strong interference in their receiver whenever the antenna beam of their transmitter was directed towards moving objects. They concluded that the variation of the received field strength must have been caused by the interference of the waves travelling towards and back from a reflecting target. Three years later, in 1925, the Americans G. Breit and M. A. Tuve were the first to use broadband pulses ranging from 3 to 30 MHz to measure the height of different layers of the ionosphere. They can be looked upon as the inventors of pulsed techniques [6], [7].

It was then only in the early thirties of the last century that the value of the radar principle was finally recognized in several countries in Europe and overseas, predominantly because of its military potential [2], [8]. In order not to go beyond the limits of this paper, the focus will be on the evolution of radar in Germany and UK. However, for historical fairness, it should be mentioned that operational radar systems were also deployed in the USA, France, the Soviet Union, Japan, Italy and in the Netherlands by the time World War II broke out in September 1939.

In 1931 Dr. Rudolf Kühnhold of the Nachrichtenmittel-Versuchsanstalt (Department of Signals Research) of the German Navy in Kiel filed a patent of what today is called SONAR for detection and ranging of objects under water by ultrasonic waves. At the same time, Kühnhold thought of using centimetre electromagnetic waves outside water for the same purpose [9], [10], [11], [12]. In order to realize those ideas, he established a new company in 1934 called GEMA (Gesellschaft für Elektroakustische und Mechanische Apparate m.b.H.) which was dedicated to the development of wireless direction finding equipment [13].

In September 1935, GEMA demonstrated an instrument in front of high-ranking Navy officials that for the first time could be named Radar, although this abbreviation had not yet been used in Germany at that time. The set consisted of a pulsed transmitter operating at a frequency of 600 MHz with an output power of 800 W. The propagation time of the pulses to and back from a target was measured to

derive the target's distance, thus adding a ranging capability to what Hülsmeyer had demonstrated 31 years before. The antennas used for transmission and reception were pine-tree arrays consisting of 10 pairs of dipoles in front of a reflecting plane. A small artillery training boat could be detected over a distance of 8 km.

In the same year Dr. Wilhelm Runge of Telefunken was working on radio links in the UHF-range. Driven by curiosity, he put the antenna of such a 600 MHz transmitter next to a second antenna connected to a detector, both positioned on the ground and pointed upwards to the sky. He managed to receive clear echoes from a Ju 52 aircraft flying past this experimental radar at a height of 5,000 m.

As a third company, Lorenz successfully tested a radar at 430 MHz with a transmitter power of 400 W on the roof of their laboratories in Berlin in 1936.

It should be added here that besides these industrial activities, significant research and development work in the radar field was being performed at that time by notable German institutions like the DVG (Drahtlostelegraphische und Luftelektrische Versuchsstation Gräfelfing) and FFO (Flugfunk-Forschungsinstitut Oberpfaffenhofen), a predecessor of today's DLR (Deutsches Zentrum für Luft- und Raumfahrt, German Aerospace Centre).

Industry and research establishments had laid the foundations for an intensive development which yielded a multiplicity of famous radar equipment. In Germany they were summarized under the synonym "Funkmesstechnik", which might be translated as "Radio Measurement Technique". In Great Britain, the term "Radio Direction Finding (RDF)" was used for reasons of secrecy from 1935 to 1943.

The Influence of Innovation Systems on Radar Development in Germany and Great Britain before and during World War II [14]

A comparison of key innovation steps between Germany and Great Britain before and during the Second World War against the background of the respective innovation systems reveals both, simultaneous developments in technologies and their applications as well as completely new innovations on the British side in the area of strategic and organizational planning on the basis of a clearly structured innovation process [15], [16]. This was present in Great Britain from the very beginning, whereas in Germany essential points of a defined innovation process were missing until the end of the war, and against the background of the successful battles on the continent within a short period of time, serious mistakes were made in technological planning, which increasingly led to the superiority of the Allies from the middle of the Second World War.

While in Germany the origin of radar development primarily originated from a demand by the Navy for an improved measuring system compared to sonic localisation, but also the ship's artillery demanded an all-weather localisation system against aircraft, in Great Britain the idea of localisation attacking aircraft by means of electromagnetic waves initially arose from the purely theoretical analysis of possible localization methods in different ranges of the electromagnetic spectrum, of which the radar idea eventually emerged as the most effective.

In both, Germany and Great Britain, it was recognised at about the same time that conventional acoustic eavesdropping methods, for example, were only of limited use for early warning of attacking aircraft, which were becoming faster and faster and could also reach higher altitudes. Although listening devices were still used in both countries during the Second World War, the radar idea dominated as a warning of attacking aircraft soon after the war began.

In Germany, optical means were still used to locate approaching aircraft in the early 1930s. At night, powerful searchlights were used, which were roughly instructed by listening devices and could reach a range of 10 km. If visibility was poor due to fog or clouds, only the inaccurate listening devices were available. Observation posts with optical equipment also continued to operate in Britain during the Second World War to assist in the reconnaissance of approaching German aircraft.

In autumn 1933, the first attempts to use the reflection of electromagnetic waves to locate targets against ships were made at the Nachrichtenmittel-Versuchsanstalt (NVA) of the Reichsmarine in Kiel [17]. Subsequently, the developments were extended to the field of air surveillance.

In Great Britain, an analysis of existing tracking systems for air defence purposes was carried out by A. P. Rowe at the British Air Ministry in June 1934 [9]. Here, too, it was firmly believed that early warning against attacking aircraft with conventional technology such as the acoustic listening devices was no longer sufficient. Likewise, Rowe ruled out air surveillance with permanently flying patrols, as these would have far exceeded the available resources of aircraft and personnel. In a memorandum, he clearly stated the need for science to find a new method to support air defence. Very quickly, against the background of a probable German threat, possible detection methods, for example using infrared technology, were investigated. But the use of barrage balloons, air mines and parachute bombs were also considered. Finally, it became apparent that the evaluation of reflected electromagnetic waves was the most effective way to defend against enemy air attacks.

Major radar developments on the German side were “Freya” by GEMA for air surveillance and early warning and later for the briefing of anti-aircraft targets with ranges of up to 150 km. In addition, “Seetakt” radar at shorter wavelengths was developed by GEMA within the framework of existing work for equipping ships, and in 1938 the armoured ship “Graf Spee” was the first ship to be equipped with a “Seetakt” radar, as the acceptance of radar for naval warfare increased considerably, especially after the start of the war.

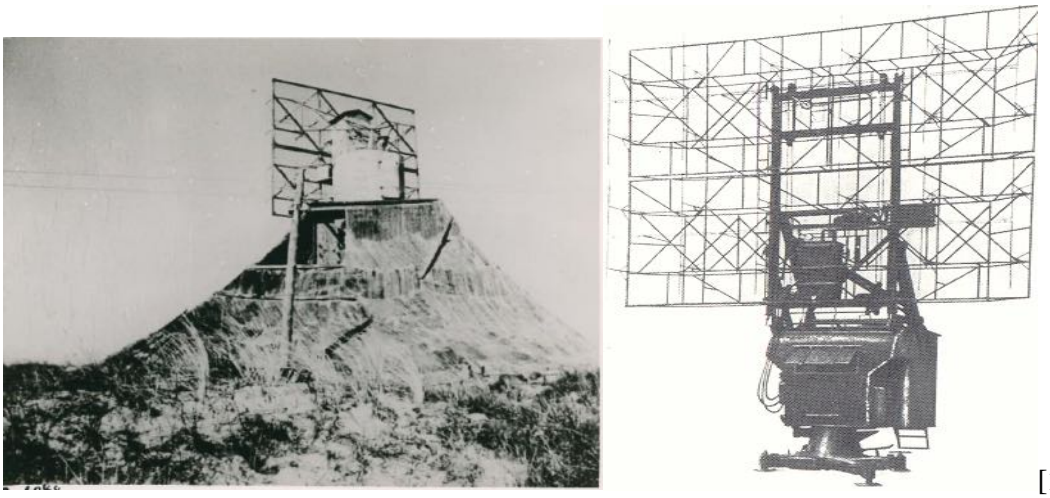

[10]

Figure 2: First stationary Freya on Wangerooge and a first series set of Freya

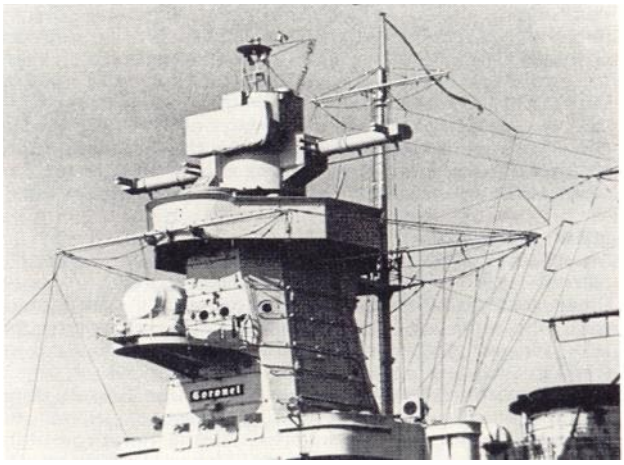

[10]

Figure 3: FuMG 38 G “Seetakt” (covered by sailcloth) mounted on the mast of the armoured vessel Admiral Graf Spee

While the focus in Germany was on the ongoing development of existing equipment, Great Britain began to develop radars for air surveillance, initially along its east coast, from 1937 onwards. These fixed “Chain Home” radar stations can be seen as a counterpart to the Freya radars. Chain Home initially operated at longer wavelengths than the Freya equipment, with correspondingly lower resolution, and at the beginning could not compete with the existing German radar equipment in its level of development [18].

Figure 4: Bawdsey Manor with Chain Home radarstation
(Source: D. Clouting, Bawdsey, Suffolk, UK)

Great Britain, on the other hand, began very early to embed the Chain Home radar stations in an integrated air defence system. In this respect, innovations were also made at the organizational and process level from a comprehensive perspective of defence against German air attacks. This included the codebreakers at Bletchley Park, radio direction finding and the introduction of “operational research”, which was completely unknown in Germany [19], [20]. The development of a comprehensive concept for air defence was only made possible by the close and unbureaucratic cooperation of all those responsible in politics, the military, science and industry.

After the beginning of the Second World War, seven Freya radars and four naval radars were delivered by GEMA by the end of 1939. The first Freya radar unit was already set up in the spring of 1939 after the German invasion of Czechoslovakia for air surveillance. The seven Freya devices were set up on islands along the North Sea coast. By the end of the Second World War, more than 2,000 Freya units had been produced in a wide variety of further developments.

At the time of the declaration of war on Germany on 3 September 1939, 18 Chain Home radar stations in Great Britain were already operational and integrated into a comprehensive networked information system, the so-called “Filter Room” with clear command structures.

In the period that followed, German radar developments focused both on a large number of variants of existing equipment and on new developments for long-range air up to a distance of 300 km. In March 1939 Telefunken introduced "Würzburg", an anti-aircraft artillery radar with an instrumented range up to 30 km. These radars with the name Würzburg were built in many variations. In total, a series of 4,000 Würzburg sets were built until the end of the Second World War. In order to support Freya in guiding fighter aircraft, "Würzburg Giant" was established as tracking radar with a reflector of 7,4 m diameter and an increased range of up to 70 km [2], [21].

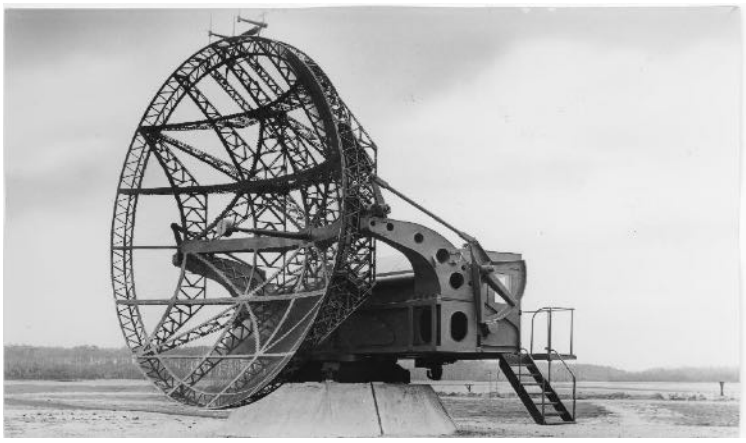 [2]

Figure 5: Anti-Aircraft Artillery Radar Würzburg Giant

In Great Britain, on the other hand, the installation of radar equipment on board of aircraft for the detection of air and sea targets began to be investigated earlier than in Germany and the first trials were completed by the end of 1937. In the following years, 1938 and 1939, the focus was on installing radar equipment in RAF and Royal Navy aircraft and on test flights with high-ranking representatives of the Royal Air Force and Royal Navy [22]. The development of the "Cavity Magnetron" as a key technology at the University of Birmingham in 1940 resulted in an outstanding increase in performance in the technological sector in the development of high-resolution radars at a frequency of 3.3 GHz, which in turn had an extraordinary influence on the target resolution [23].

In the autumn of 1941, the Telefunken company was able to put an operational on-board radar into service for the first time in Germany, the "Lichtenstein BC (FuG 202)". This on-board radar operated at a frequency of 490 MHz and involved a cumbersome arrangement of antennas on the head of the aircraft. The "Berlin N1A" on-board radar from Telefunken for night hunting, which operated in a high frequency range like the British on-board radars were already in use since 1943 and which already had essential features of later radars with regard to the installation dimensions, was not used in small numbers until 1945.

In the course of the war, attack and defence were reversed on the German and British sides. While the emphasis on the German side was initially on attack, Germany was increasingly forced into a defensive posture in the course of the war. In Great Britain, the development was reversed. Whereas the initial focus was on defence against enemy air attacks, in the course of the war the emphasis shifted to attack.

This was also against the background of great technological progress in the development of British radar equipment, which operated in the centimetre wave range with high performance. The corresponding milestone in technological progress was the invention of the Cavity Magnetron in 1940, which now made it possible to generate very high power in the centimetre wave range. This radical innovation made it possible to install high-resolution radar units with correspondingly greatly reduced installation dimensions in aircraft. This made it possible to bomb German cities with pinpoint accuracy and to fight German submarines effectively. Furthermore, innovation cooperations played a major role in progress in the development and production of technologically advanced radar equipment. The main focus was on cooperation between Great Britain and the United States in the field of centimetre-wave technology. The mission of British scientists with the latest technological findings to the United States in 1940, the so-called "Tizard Mission", was a prime example of a trusting cooperation between scientists and industry in both countries [24]. Germany was unable to counter this technological breakthrough. In addition, there was a clearly developed concept in Great Britain for the central networking and evaluation of all information obtained from air surveillance.

Resurgence of Radar after World War II

At the end of World War II radar development in Germany came to a complete stop. Any research work in this field was prohibited by the Allies until 1950. Nevertheless, basic architectures of radar systems had been evaluated, the principles of pulse- and continuous wave (CW)-radars and their applications for surveillance and target tracking were established and understood. This was a sound basis for a re-start of a new German radar industry to come.
Mainly in the US radar development proceeded significantly after the war. The area of coherent system operation and Doppler signal processing, for instance, saw many advances. On the other hand, high-power klystron tubes for the first time enabled coherent locking of a receiver to the transmitted pulse yielding first MTI-systems to go into operation. Further, the new technique of pulse compression had been combined with coherent Doppler signal processing to achieve fine resolution both in range and Doppler. Another important innovation in tracking radar technology was the monopulse tracking system. In parallel to all theoretical work the increasing availability of new technologies, only to mention semiconductors or microprocessors, were keys for the radar evolution [2].

By 1945, many industrial facilities in Germany were destroyed or later dismantled, with the employees scattered all over the post-war country. As an example of the electronic industry, the Telefunken company shall be looked at in the following. Here, soon some work was restarted on a small scale and by 1946 production of radios and radio transmitters was re-established at factories in Berlin and Dachau. However, activities in the frequency range above 100 MHz, and especially in the field of radar, were forbidden under the laws of the Allied Military Government**.** German companies were first allowed to build British radar equipment on a licence basis in 1950, e.g. for civil air traffic control or maritime surveillance applications [1].

In 1955, in the frame of the so-called “Paris Treaties” between the Western Allies and the German Federal Republic, all limitations for work on radar in Germany were lifted and national developments became possible. With the beginning of the Cold War and West German rearmament within NATO, it was expected that military radars would also be needed again, but military equipment could not be built in Berlin under the “Four Power Status” of that city, which lasted until 1989. The Telefunken “Radar Department” was therefore transferred to Ulm in 1957, where a factory for HF electronics already existed. Thus, Ulm became the final location of Telefunken Radar.

Ground Radars

In 1954, the newly founded Air Traffic Control Authority of the German Federal Republic, the BFS (Bundesanstalt für Flugsicherung), decided to procure a GCA (Ground Controlled Approach)-system from the US company Bendix for the German civil airports. The system, consisting of the “Airport Surveillance Radar ASR-3” and the “Precision Approach Radar PAR-2”, had been newly developed by Bendix according to CAA (Civil Aeronautics Administration)-specifications and had just been introduced in the USA. Telefunken succeeded in getting a licence contract from Bendix for the production of the German equipment as well as obtaining a production permit from the Allied authorities.

The ASR-3 Airport Surveillance Radar was designed for a 50 NM coverage around the airport. The cosec^2-elevation diagram provided a constant height coverage up to 5 km. The magnetron transmitter was tuneable to a fixed frequency between 2.7 and 2.9 GHz with a peak output power of 500 kW and a pulse length of 1 µs [1].

 [1]

Figure 6: ASR-3 tower

Shipborne Radar

One of the first modern shipborne radars finally becoming a standard equipment of the German Navy was “TRS-N”. After being developed by Telefunken in the fifties of the last century, a number of 69 sets have been delivered. TRS-N was a dual-band system with switchable frequencies of 5.5 and 9.5 GHz. For both frequencies one common antenna system with a parabolic reflector was used. The radar was mostly used for smaller units of the Navy, such as boats for mine-hunting [2].

 [2]

Figure 7: Shipborne radar TRS-N

Airborne Radar

Military airborne radars for fighter applications are one of the technical drivers in the radar field. The quantum leap in fighter radar development appeared in the transition from the „analogue“ to the „digital“ radar. “NASARR (North American Search and Ranging Radar)” is one of the last representatives of an analogue fighter radar used in the F-104 Starfighter. This is, last but not least, indicated by the fact that no less than 267 potentiometers had to be set manually to calibrate the radar. NASARR was produced from 1961 to 1966.


[2]

Figure 8: Airborne radar NASARR for fighter aircraft F-104 Starfighter

The important step to digital radar was initiated in the mid sixties. The result were radars with almost all system parameters being controlled by software. “APG-65” for the F-4 Phantom was one of the first digital radars. The „Tornado Nose Radar (TNR)“ can moreover be entitled a digital multifunction radar. Different operation modes are available controlled by the radar processor like air-to-surface mapping, air-to-surface attack or terrain following during low level flight [2].

Conclusion

The basics of radar development since the beginning of the 20th century have been shown in this paper. A predominant aspect demonstrated is the different philosophy of research and development in Germany and Great Britain against the background of innovation systems especially prior and during World War II. The new entry into radar developments in Germany has been described until about the sixties of the last century.

Looking into the future, one of the main features of high performance radars is “Synthetic Aperture Radar (SAR)” [25]. SAR was initially introduced by C. Wiley of Goodyear Aircraft Corporation in June 1951. He postulated that extremely high angular resolution of a radar could be achieved by frequency analysis of the received signal of a coherent radar. This is the basic feature of SAR.

References

[1] Holpp, W., Speck, R., Daembkes, H. (Editors): *60 Years of Radar Technology in Ulm.* Eberl Print, Immenstadt, 2014

[2] Holpp, W.: *The Century of Radar*. In: 100 Years of Radar, Special Issue, DGON, Bonn, 2004. pp. 171 - 200

[3] Bauer, A. O.: *Christian Hülsmeyer and the Early Days of Radar, Sense and Nonsense.* In: 100 Years of Radar, Special Issue, DGON, Bonn, 2004, pp. 14 - 58

[4] Marconi, G.: *Wireless Telegraphic Communication.* Nobel Lecture, December 11, 1909, https://www.nobelprize.org/prizes/physics/1909/marconi/lecture/

[5] Bussey, G.: *Marconi´s Atlantic Leap*. Marconi Communications, Coventry, 2000

[6] Holpp, W.: *Die Geschichte der Radarmesstechnik*. In: Geschichte der elektrischen Messtechnik, Geschichte der Elektrotechnik 25, VDE Verlag, Berlin, 2014, pp. 177-214

[7] Buderi, R.: *The Invention that Changed the World: How a Small Group of Radar Pioneers Won the Second World War and Launched a Technological Revolution*. Simon and Schuster, New York, 1996, pp. 61 - 62

[8] Blumtritt, O. et. al. (Editor): *Tracking the History of Radar*, IEEE-Rutgers Center for the History of Electrical Engineering and the Deutsches Museum, Piscataway,1994

[9] Reuter, F.: *Funkmeß. Die Entwicklung und der Einsatz des RADAR-Verfahrens in Deutschland bis zum Ende des Zweiten Weltkrieges*. Wissenschaftliche Abhandlungen der Arbeitsgemeinschaft für Forschung des Landes Nordrhein-Westfalen, Band 42, Springer, Wiesbaden, 1971

[10] Trenkle, F.: *Die deutschen Funkmessverfahren bis 1945*. Motorbuch, Stuttgart, 1979

[11] Kümmritz, H.: *On the development of radar technologies in Germany up to 1945*. In: Tracking the History of Radar, IEEE-Rutgers Center for the History of Electrical Engineering and the Deutsches Museum, 1994, pp. 25 - 46

[12] Swords, S.S.: *Beginning of radar in Germany*. In: Technical History of the Beginnings of Radar. The Institution of Engineering and Technology, London, 2008, pp. 91 - 101

[13] Kroge, H. v.: *GEMA – Berlin. Geburtsstätte der deutschen aktiven Wasserschall- und Funkortungstechnik*. Lüthmanndruck, Hamburg-Harburg, 1998

[14] Klausing, H.: unpublished manuscript, 2022

[15] Watson-Watt, R.: *Three Steps to Victory*. Odhams Press Limited, London, 1957

[16] Zimmerman, D.: *Britain´s Shield and the Defeat of the Luftwaffe*. Amberley Publishing, Gloucestershire, 2013

[17] Rowe, A.P.: *One Story of Radar*. Cambridge University Press, Cambridge, 1948

[18] Dobinson, C.: *Building Radar. Forging Britain´s early-warning chain, 1935 - 45*. Methuen, 2010

[19] Rohwer, J; Jäckel, E. (Hg.): *Die Funkaufklärung und ihre Rolle im Zweiten Weltkrieg*. Motorbuch, Stuttgart, 1979

[20] Jones, R.V.: *Most Secret War. British Scientific Intelligence 1939 - 1945*. Penguin Books, London, 2009

[21] Trenkle, F.: Die deutschen Funkmessverfahren bis 1945. Hüthig, Heidelberg, 1986, pp. 46 - 49

[22] Bowen, E. G.: *Radar Days*. Adam Hilger, Bristol, 1987

[23] Redhead, P.A.: *The Invention of the Cavity Magnetron and its Introduction into Canada and the U.S.A.* In: La Physique au Canada, Nov./Dec. 2001, pp. 321 - 328

[24] Phelps, S.: *The Tizard-Mission. The Top-Secret Operation that Changed the Course of World War II*. Westholme Publishing, Yardley, Pennsylvania, 2010

[25] Klausing, H., Holpp, W. (Editors): *Radar mit realer und synthetischer Apertur*. Oldenbourg, München, 2000

Dr.-Ing. Wolfgang Holpp
Am Nohl 72
89173 Lonsee
Germany

Wolfgang.Holpp@gmail.com

Dr.-Ing. Wolfgang Holpp has been working for HENSOLDT AG and a number of predecessor companies until the end of 2018.
He studied electrical engineering at the University of Stuttgart and received his doctorate in 1985 with an investigation of dielectric filter structures for short millimeter wavelengths. At the same time he was head of the microwave and millimeterwave components laboratory at former AEG-TELEFUNKEN. Later he was technical project manager of a microwave data link for a RPV application, several radar seeker heads for missile guidance and finally of the pre-development of the Active Electronically Scanned Array Radar for the Eurofighter aircraft. In 2003 he was appointed Senior Manager.
Dr. Holpp has been teaching at the Ulm University of Applied Sciences, the Bundesakademie für Wehrverwaltung und Wehrtechnik (Federal Academy of Defence Administration and Technology) in Mannheim and the Carl-Cranz-Gesellschaft, where he was also chairman of the board from 2015 until 2018. He has published more than 80 papers for professional journals and symposia contributions. Together with Prof. Klausing he is editor and co-author of the book „Radar mit realer und synthetischer Apertur“ (2000). In 2014 he co-edited the book „60 Years of Radar Technology in Ulm“.

Prof. Dr.-Ing. Helmut Klausing
Am Drössel 8
82234 Weßling
Germany

Helmut.Klausing@t-online.de

Prof. Dr.-Ing. Helmut Klausing has been President of GPM Deutsche Gesellschaft für Projektmanagement e.V. (German Association for Project Management) from 2016 until the end of 2020. From 2006 to the end of 2015, he was member of the Board of the VDE Verband der Elektrotechnik Elektronik Informationstechnik e.V. (Association for Electrical, Electronic & Information Technologies).
After studying electrical engineering and gaining his doctorate in the field of high-resolution radar technology in 1989, he worked as a project manager and executive at Siemens AG and EADS Deutschland GmbH. He had business responsibility over several locations in Germany and internationally in the fields of traffic engineering, mobile communications and aviation.
Prof. Klausing teaches as an honorary professor in the field of innovation management and industrial processes at the Karlsruhe Institute of Technology (KIT).
For many years he has been studying the history of radar technology with a focus on Germany and Great Britain in cooperation with the co-author W. Holpp.

Back to table of contents

A freely usable mission control system for mountain rescue operations based on satellite navigation, live tracking and geoinformation data

Marco Gabl, Institute of Geography, University of Innsbruck

Abstract:
A coordinated and effective approach is vital for mountain rescue operations. The time factor is the key challenge in accidents in alpine regions, in the search for missing persons or in natural disasters such as avalanches. The Assisted Rescue Control System (ARCOS) developed at the Institute of Geography at the University of Innsbruck focuses precisely on this circumstance: rapid and efficient organizational support during emergency operations. Since the completion of the mission control system, more than 150 missions and additionally numerous exercises and trainings have been carried out at the mountain rescue base Bergrettung Oberes Drautal, Carinthia in Austria. The key aspects of this system are satellite-based real-time tracking of the emergency forces, navigation with the help of (photorealistic) 3D mission maps and geoinformation data.
Keywords: Live tracking, GNSS, Mountain rescue

1. Introduction

The development of ARCOS was aimed at increasing the operational efficiency of the mountain rescue organization. Thus, a mission control system was created that meets the requirements of a voluntary alpine rescue organization. The goal of any search and rescue (SAR) mission is to locate the missing or injured subject and return them to a stable and safe environment (FERGUSON 2008). A SAR mission is a complex process that often must be conducted without complete information and adequate resources. Therefore, it is highly important to plan and coordinate SAR operations effectively (WYSOKIŃSKI et al. 2014). In disaster response, it is important that decision makers have correct and relevant information in a timely manner (HANSSEN 2018).

Figure 1: Night SAR operation (archive BRD Oberes Drautal, 2021)

The focus is on improving the coordination of rescue forces and situational awareness. The application of the incident command system is intended to reduce the time required to rescue or locate an injured person and moreover to ensure the safety of the rescue team. ARCOS has a lean and robust system architecture, is characterized by a very simple and intuitive handling and is supplemented with free geodata. The program is free of software and licence costs - a system by and for volunteer rescue organizations. This paper presents the mission control system and discusses the application of geodata, simple GIS functionalities in combination with real-time data using the example of mountain rescue missions.

2. System structure

The rescue team is coordinated by satellite-based positioning from a central mission control centre. An essential component is the transmission of the real-time position data of the mountain rescuers to the mission monitoring system. This is handled with robust GNSS trackers. The position coordinates are sent to a tracking portal via the mobile network or the Internet, and the position data is simultaneously transmitted to the personalized operation centre (Fig. 1). If there is no network coverage in an area, the location coordinates are temporarily stored at the GNSS trackers internal storage and forwarded to the centre when they are received again. This ensures that no position data is lost. In addition, the rescuers are equipped with radios as a backup to be able to communicate with the control centre.

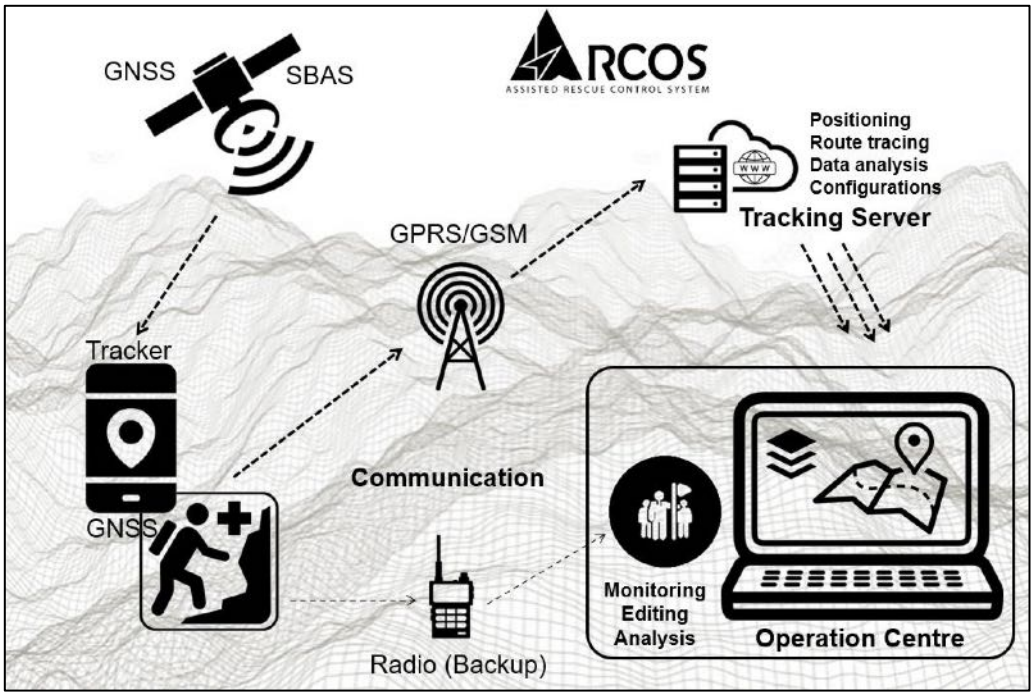

Figure 2: System Architecture (own illustration, 2022)

2.1 GNSS-Tracker & Positioning

The mobile GNSS trackers provide the current position of the crew in the field and are thus a main component of the present system. The GNSS trackers used (awtraxx® Finder Mini) are a combination of a GNSS receiver and a GSM/GPRS module for live data transmission. For positioning, the constellations GPS and Glonass in single-point

position mode are used (L1; C/A) as well as SBAS. Assisted GPS (A-GPS) is utilized for a faster initialization time (time to first fix). Since search and rescue operations often take place in alpine regions or in forest areas, the topography or the canopy can cause increased signal interference with the trackers. The use of multi-GNSS capable devices is therefore advisable. New and modernized signals of the lower L-band (e.g. L5/E5) offer improved multipath rejection and greater robustness against interference as well as more robust tracking even at weak signal strengths (MONTENBRUCK et al. 2004). In addition, the use of multi-frequency receivers is the most effective way to largely eliminate ionospheric interference. When these advantages of the lower L-band are combined with the ability to minimize ionospheric errors, significant improvements in positioning accuracy can be achieved (JEFFREY 2010). Smartphones with multi-GNSS capable chipsets are well suited for this purpose and can be integrated into the present system.

2.2 Tracking portal

The position data (coordinates, speed, heading, time indication), battery and satellite status are sent from the GNSS trackers to an internet based tracking portal (Fig. 2). The portal has several interfaces to implement the data into different programs. The use of single devices up to more complex fleet management is supported. In addition to a variety of commercially available trackers, smartphones are also provided. In the tracking portal, the most important information, such as the graphical display of the real-time position, route display, time-based selection, export and storage of the data are offered. The web-based portal is suitable for a quick situation overview for incident commanders on their tablets or smartphones while on the move. A data interface enables the transfer of real-time data from the tracking portal to the cockpit. The full range of functions is provided in the actual core system, the operations cockpit (2.3), for which an IT infrastructure with at least a laptop or PC and Internet connection must be available.

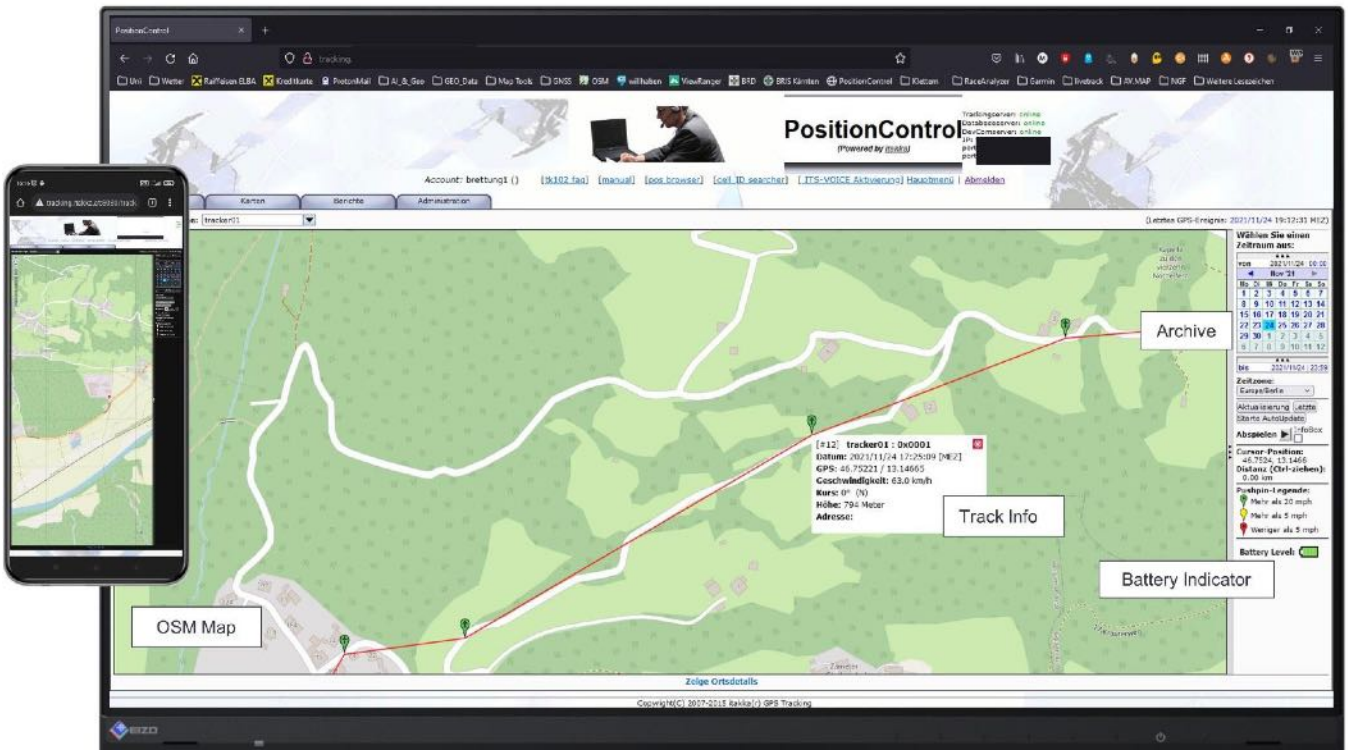

Figure 3: Web-based tracking portal (own illustration & data, 2022)

2.3 Monitoring cockpit

The base of any SAR mission is a (topographic) map. GIS - functionalities become indispensable tools for every aspect of SAR by creating maps for visualization and analysis of the terrain so that the mission command and field teams can keep track of a continuous stream of information (DURKEE, & GLYNN-LINARIS, 2012).

With the help of the operations cockpit, rescue operations are handled. The system itself, is essentially based on the free software Google Earth Pro and modified for search and rescue operations. Although Google Earth is not a full-featured GIS, the software enables essential functions such as visualization, overlay and creation of geospatial data. In addition to a quick and intuitive learning curve, the monitoring cockpit is also used to overlay high-resolution orthophotos of the Länderkooperationen (GEOLAND.AT). Additionally it provides the visualization of topographic map layers. Licensed maps from the Bundesamt für Eich- und Vermessungswesen (ÖK50) and maps from Kompass Verlag are used. In addition, the free Open Street Map and the Verwaltungsgrundkarte von Österreich (BASEMAP.AT) are used, which with its high-resolution hillshading is a valuable resource for operations. For avalanche operations, Google Earth was modified with slope maps derived from a five-meter resolution terrain model. Specially prepared data sets, such as the visualization of bike park routes, helipads, hazard zone maps or a mobile network coverage map for the area of operation are also available.

Adaptation of the cockpit to the requirements of the individual operational organization can thus be implemented. In addition, simple editing functions such as the delimitation of a search area or the import and export of GPX tracks are possible. There is an option to perform live tracking and navigation using smartphones. Another useful feature is the automatic archiving of deployments. Thus, all missions are saved and mission statistics are calculated, which is of great value for debriefings.

Figure 4: Monitoring cockpit (own illustration & data, 2022)

3. Results and discussion

The experiences of the last years show that the use of the Assisted Rescue Control System has positive effects on the situation control during mountain rescue operations. The advantages of a real-time based mission control system are efficient and effective coordination of the rescue team in alpine terrain. Similar results were also found by GEORGOPOULOS et al. (2010), LEE et al. (2017) and PRÜLLER et al. (2015). Not only is valuable time saved, but monitoring also increases the safety aspect for the rescue team itself, for example when rescuers drift into dangerous terrain due to weather conditions and can thus be warned at an early stage. These positive results are further enhanced by the use of photorealistic 3D maps. With the help of the mission maps, it is possible to capture and interpret the terrain and situation in the best possible way. The resulting overview of the operation, taking into account relevant geodata, such as the slope gradient in avalanche operations, makes it possible to reinforce the necessary arguments for decision-making. By documenting operations or exercises, the mission control system can be used to analyse demonstrative scenarios that can be helpful in planning future scenarios. The user-friendly handling of the program means that even non-specialists can operate the mission control system properly after a short training phase. Specially trained and assigned personnel are not necessary. During the development, the cost factor was also taken into account. The monitoring system was developed entirely independently and without external financing, it is freely available and of charge, which is a novelty in this sector.

Marco Gabl, MSc. is a research associate and PhD candidate at the Department of Geography at the University of Innsbruck. He mainly focuses on data acquisition with mobile GIS, remote sensing data, deep learning in the context of Geographic Information Systems (GeoAI). He developed the mission control system ARCOS for mountain rescue missions and does research in this topic.

Institut für Geographie
Universität Innsbruck
Innrain 52f
6020 Innsbruck, Austria
marco.gabl@uibk.ac.at

References

BASEMAP.AT, Verwaltungsgrundkarte von Österreich. https://basemap.at.

DURKEE, G. & GLYNN-LINARIS, V. (2012). Using GIS for wildland search and rescue.

FERGUSON, D. (Hrsg.) (2008), GIS FOR WILDERNESS SEARCH AND RESCUE, Washington, D.C.

GEOLAND.AT, Kostenloses Geodatenportal der österreichischen Länder. https://www.geoland.at.

GEORGOPOULOS, P., MCCARTHY, B. & EDWARDS, C. (2010), Location Awareness Rescue System : Support for Mountain Rescue Teams. Computing Department, InfoLab21.

HANSSEN, Ø. (2018), Position Tracking and GIS in Search and Rescue Operations. In: TITKO, M., RISTVEJ, J. & HOLLA, K. (Hrsg.), Crisis Management - Theory and Practice. IntechOpen, doi: 10.5772/intechopen.75371.

JEFFREY, C. (2010), An introduction to GNSS. GPS, GLONASS, Galileo and other Global Navigation Satellite Systems. 1st ed. Calgary: NovAtel.

LEE, S.-H., NI, J.-C., ZHAO, Y.-G. & YANG, C.-S. (2017), A real-time emergency rescue assistance system for mountaineers. In: 2017 IEEE International Conference on Consumer Electronics (ICCE). IEEE, 106–107, doi: 10.1109/ICCE.2017.7889245.

MONTENBRUCK, O., TEIGENBERGER, P., KHACHIKYAN, R., WEBER, G., LANGLEY, R. & MERVART, L. & HUGENTOBLER, U. (2004), IGS-MGEX Preparing the Ground for Multi-Constellation GNSS Science. https://www.insidegnss.com/auto/janfeb14-MONTENBRUCK.pdf.

PRÜLLER, R., FÖSTLEITNER, C. & SOMMER, C. (2015), SARONTAR – ein Einsatzleitsystem für Notfälle in alpinen Regionen. In: STROBL, J., BLASCHKE, T., GRIESEBNER, G. & ZAGEL, B. (ed.), Angewandte Geoinformatik 2015. Beiträge zum 27. AGIT-Symposium Salzburg. Wichmann, H, Berlin, 252–257.

WYSOKIŃSKI, M., MARCJAN, R. & DAJDA, J. (2014), Decision Support Software for Search & Rescue Operations. In: Procedia Computer Science, 35, 776–785, doi: 10.1016/j.procs.2014.08.160.

Back to table of contents

Earth observation-based assessment of mass movement impact on alpine infrastructure management

Florian Albrecht[1], Daniel Hölbling[1], Lorena Abad[1], Zahra Dabiri[1], Gerald Reischenböck[2]

[1] Department of Geoinformatics - Z_GIS, University of Salzburg, Salzburg, Austria

[2] MJP Ziviltechniker GmbH, Gmunden, Austria

Email: {florian.albrecht, daniel.hoelbling, lorena.abad, zahra.dabiri}@plus.ac.at; g.reischenboeck@mjp-zt.at

Abstract

Gravitational mass movements and erosion are among the main natural processes that affect the durability of alpine infrastructure. Earth observation and geoinformation technologies allow mapping and modelling of mass movement information and assessment of the impact on alpine trails and huts. Therefore, they have the potential to support alpine infrastructure management. This study presents maps created for this purpose, including mass movement inventories, slow slope movements, mass movement susceptibility, rockfall, and erosion activity, as well as maps that assess their impact on alpine infrastructure. A validation workshop with trail keepers confirmed the potential usefulness of the maps in practice.

Introduction

The alpine infrastructure of trails and huts is a strong asset for summer tourism in the Austrian Alps. Maintaining alpine infrastructure is expensive and demanding for the Alpine associations. Natural processes, such as precipitation and runoff, constantly cause erosion of trails. In addition, geohazards such as landslides, mudflows and rockfalls repeatedly cause damage to trail networks and hut infrastructure (Figure 1). Where they occur, they may cause temporary closure of popular hiking routes, difficulty in accessing huts, or damage water supply lines and other infrastructure facilities of huts. Two current trends reinforce this dynamic: first, the strain on alpine infrastructure increases as user numbers rise with the popularity of hiking; and second, climate change causes more frequent and intense heavy rainfall. Consequently, more erosion problems occur and more damage events are expected due to the increase in triggered mass movements. The trail keepers of Alpine associations are confronted with an increasing maintenance effort for alpine infrastructure and therefore need suitable and reliable information on mass movements and erosion (Albrecht et al., 2020). Only few studies have addressed the topic of mass movements and their interaction with alpine infrastructure, for example, focusing on study areas in Italy (Raso et al., 2019) and Nepal (Jones et al., 2020). The need for a better coverage of the topic with a particular focus on Austrian study areas motivated this research.

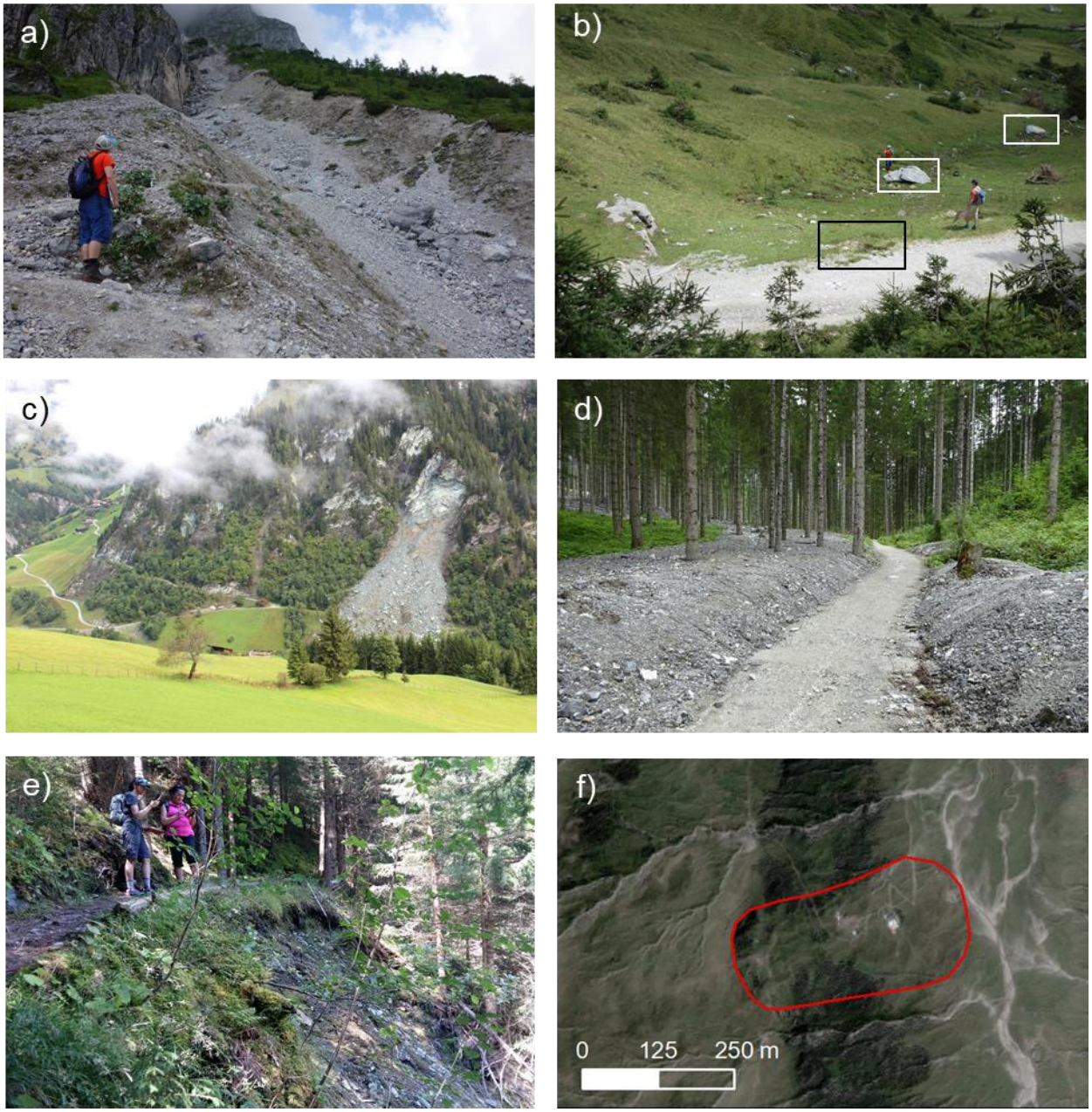

Figure 1: Examples of mass movements and erosion processes with an impact on alpine infrastructure: a) erosion that affects a trail crossing a ditch, b) falling rocks – two rocks on a pasture as candidates for causing a hit mark next to a path, c) large rockfall that destroyed trails, d) a trail dug out from a debris flow, e) shallow landslide beneath a trail, and f) deep-seated landslide where slow creeping affects the hut in its centre and infrastructure facilities in the vicinity. Photos: F. Albrecht, 2021 (a, b and e), L. Abad, 2019 (c), D. Hölbling, 2017 (d). Map data: Pleiades (f).

Earth observation (EO) methods and technologies and geospatial methods for mapping and modelling mass movements can support this need (Albrecht et al., 2020). In response, the project MontEO ("The impact of mass movements on alpine trails and huts assessed by Earth observation (EO) data") aims to exploit satellite imagery and digital elevation models (DEMs) to obtain practice-oriented information on mass movements for alpine infrastructure management. In this article, we present the requirements analysis and EO-based techniques for information extraction, mass movement modelling and impact assessment. We show the results, particularly maps of mass movements and their impact on alpine infrastructure, and discuss their usefulness in practice.

Methods

First, we analysed the needs and requirements of alpine infrastructure management for information on mass movements. Second, we identified mass movements using optical satellite data to supplement existing inventories from authorities, and synthetic aperture radar (SAR) data to identify slow slope movements. Third, we modelled mass movement susceptibility, rockfall and erosion activity. Fourth, we assessed their impact on alpine infrastructure. Fifth, we performed a validation with trail keepers to evaluate the usefulness of the map results in practice.

In the user requirements analysis, we followed the approach of Albrecht et al. (2016) and is described in more detail in (Albrecht et al., 2020). We prepared a guideline questionnaire for semi-structured interviews. We performed 12 (group) interviews with 19 interview partners who identified themselves as trail officials, trail keepers and hut keepers (with trail keeping duty), and discussed an initial concept of mass movement and impact information to support alpine infrastructure management with them. Based on the interview protocols, we identified the roles of users, their tasks and scenarios of use. Furthermore, we investigated the need for information about mass movements and their impact on alpine infrastructure. The interviews provided a vast number of cases where mass movements and erosion caused damage to alpine infrastructure. We linked them to activities that deal with the damage to alpine infrastructure and the resulting efforts to cope.

The user requirements guided us to prepare diverse maps of mass movement information and alpine infrastructure assessments in Austrian study areas in Salzburg, Upper Austria and Tyrol.

Concerning mass movement inventories, we based our analysis on existing inventories from authorities. To complement these databases, we conducted a visual interpretation based on Sentinel-2 imagery (cf. Abad et al., 2022). In particular, this enabled the inclusion of additional mass movement locations in remote mountainous areas that were not present in the inventories of the authorities. The combined inventory data were used as the basis for calculating mass movement hotspots and as inputs for susceptibility mapping.

Furthermore, we used very high-resolution Pléiades satellite images to semi-automatically extract land use and land cover (LULC) maps with object-based image analysis (OBIA) techniques. The LULC maps were used as input for modelling of rockfall and erosion. Identification of slow slope movements and surface deformation velocity was done by applying persistent scatterer interferometry (PSI). PSI is a specific differential interferometric synthetic aperture radar (DInSAR) technique which allows measurements in the range of millimetres (Crosetto et al., 2016). We used more than 30 freely available Sentinel-1 SAR images to detect slow slope movements to complement the interpretation based on optical imagery and obtain a more complete picture of the different mass movements in our study areas.

To assess the mass movement susceptibility of alpine trails and huts, we applied and compared two statistical methods, i.e., logistic regression and informative value. Besides the mass movement inventories and alpine infrastructure data derived from OpenStreetMap (OSM), nine conditioning factors (terrain derivatives, landscape and geological factors) were used for susceptibility mapping. Details on the mass movement susceptibility mapping and the performance of the two methods can be found in Abad et al. (2022).

Furthermore, we modelled rockfalls based on a DEM using a probabilistic, process-based rockfall trajectory model that combines physically-based deterministic algorithms with stochastic approaches (Mateos et al. 2016). Rockfall may set loose from slopes above a certain slope. For each location, the model estimates the probability that a falling rock will reach that location. The LULC map was included as a dampening parameter affecting the bounce of a rock.

In addition, as a proxy for erosion activity, we prepared a hydrological runoff model with functions available in GIS software on the basis of the DEM with one meter resolution derived from airborne laser scanning that is freely available for Austria.

As an alpine infrastructure assessment, the mass movement information derived from the EO data and the modelled susceptibility, rockfall reach probability, and runoff were overlaid with alpine infrastructure data derived from OSM. The mean susceptibility was calculated for a buffer of 10 m around each trail segment and of 50 m around each alpine hut. The rockfall reach probability was analysed for each location within 10 m of the trails. Additionally, possible alternative routes were digitized on an orthophoto in an area where a trial is affected by strong erosion.

The final maps were presented to trail keepers in an online questionnaire and during a dedicated validation workshop and discussed for their usefulness in practice in the context of the scenarios identified during the requirements analysis.

Results

The types of mass movements, their consequences for alpine infrastructure, and the infrastructure management tasks that address them are presented in Figure 2. The case types mostly concerned damages to trails, bridges and huts, which are caused by erosion, rockfalls, shallow landslides, debris flows, deep-seated landslides, and other issues. The cases require different tasks to follow. In case of small but frequent damages, recurring repairs are necessary at the beginning of each hiking season. Renovations are necessary occasionally when the damage is larger or has accumulated. Tasks with high costs occur rather seldom, e.g. when a route needs to be replaced due to persistent problems or when a bridge was destroyed by a debris flow.

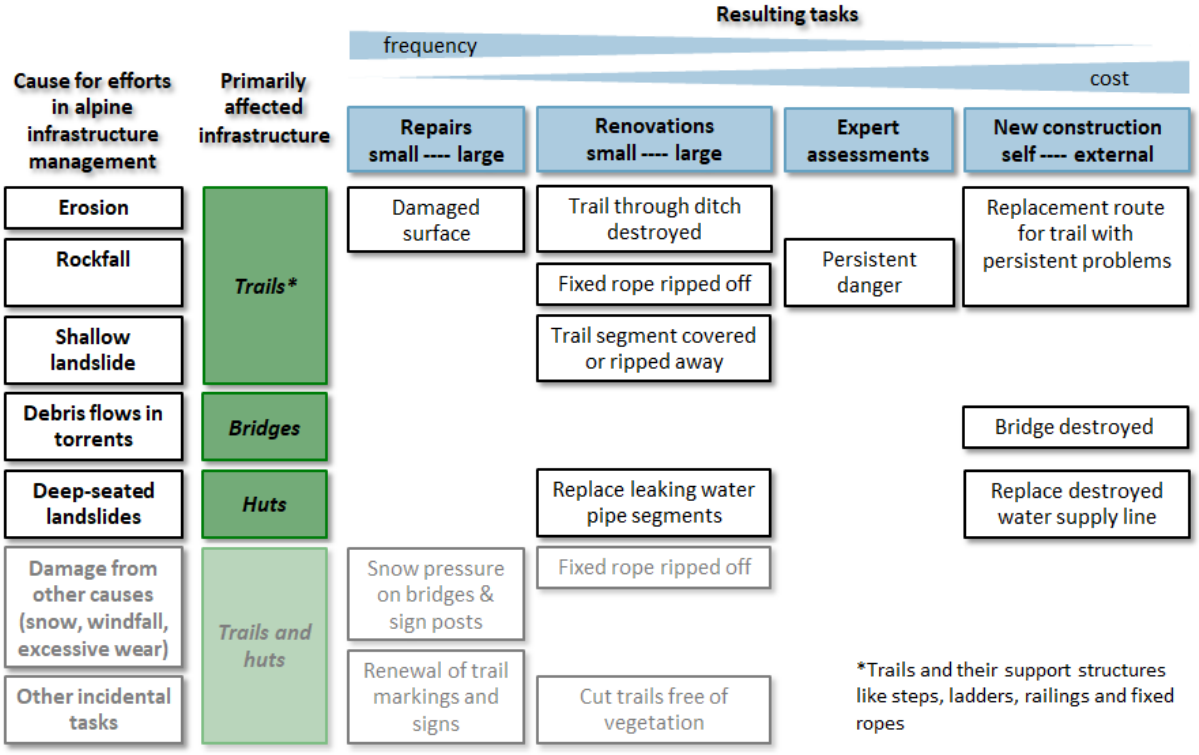

Figure 2: Mass movements and erosion as causes of damage and resulting tasks in alpine infrastructure management.

For supporting alpine infrastructure management with EO-based mass movement information and impact assessments, we identified a set of six specific application scenarios that were grouped into three general scenarios presented in Table 1.

Table 1: Scenarios (Sc) of application in alpine infrastructure management.

Scenario Number	General Scenario	Specific Scenario
Sc1	Strategic effort planning	
Sc1.1		Modelling expected costs of trail maintenance effort
Sc2	Alpine infrastructure project planning	
Sc2.1		Planning trail adaptations to counter the impact of mass movements
Sc2.2		Estimate costs of trail adaptation projects that include costs related to mass movements
Sc2.3		Planning relocation of trails to avoid mass movement impact
Sc2.4		Planning hut infrastructure to adapt for the impact of mass movements
Sc3	Management of trail closures	
Sc3.1		Authorizing trail usage at critical locations with potential risk

For the scenarios, the users need information about locations where mass movements occurred in the past and locations of slow slope movements where mass movements and erosion are ongoing. Furthermore, they need information about locations where mass movements and erosion potentially occur. Finally, they require information where trails and huts are potentially impacted by mass movements and erosion. The maps were designed to serve these information needs. Figure 3 presents the mass movement information derived from EO data. It includes a background map, amass movement inventory, a LULC map and a map of slow slope movements derived with PSI analysis.

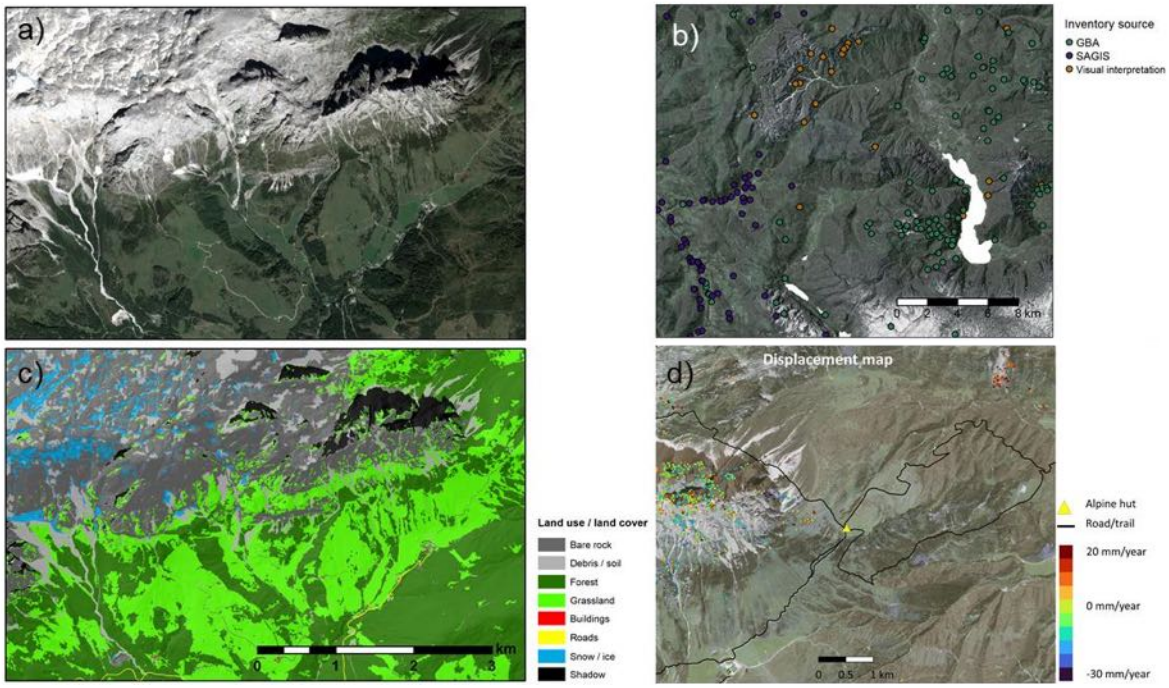

Figure 3: Digital maps about mass movements and their context derived from Earth observation (EO) data, including a) background map showing a very high-resolution Pleiades image, b) point-based mass movement inventories from existing sources and visual interpretation of optical satellite images (Sentinel-2), c) land use / land cover (LULC) maps, and d) point-based displacement maps from PSI analysis.

The comprehensive inventory allowed the identification of hotspot regions that highlight clusters of mass movements. The susceptibility maps show areas susceptible to mass movements, ranging from low to high susceptibility. The rockfall and erosion models highlight areas susceptible to rockfall or runoff-related erosion (Figure 4).

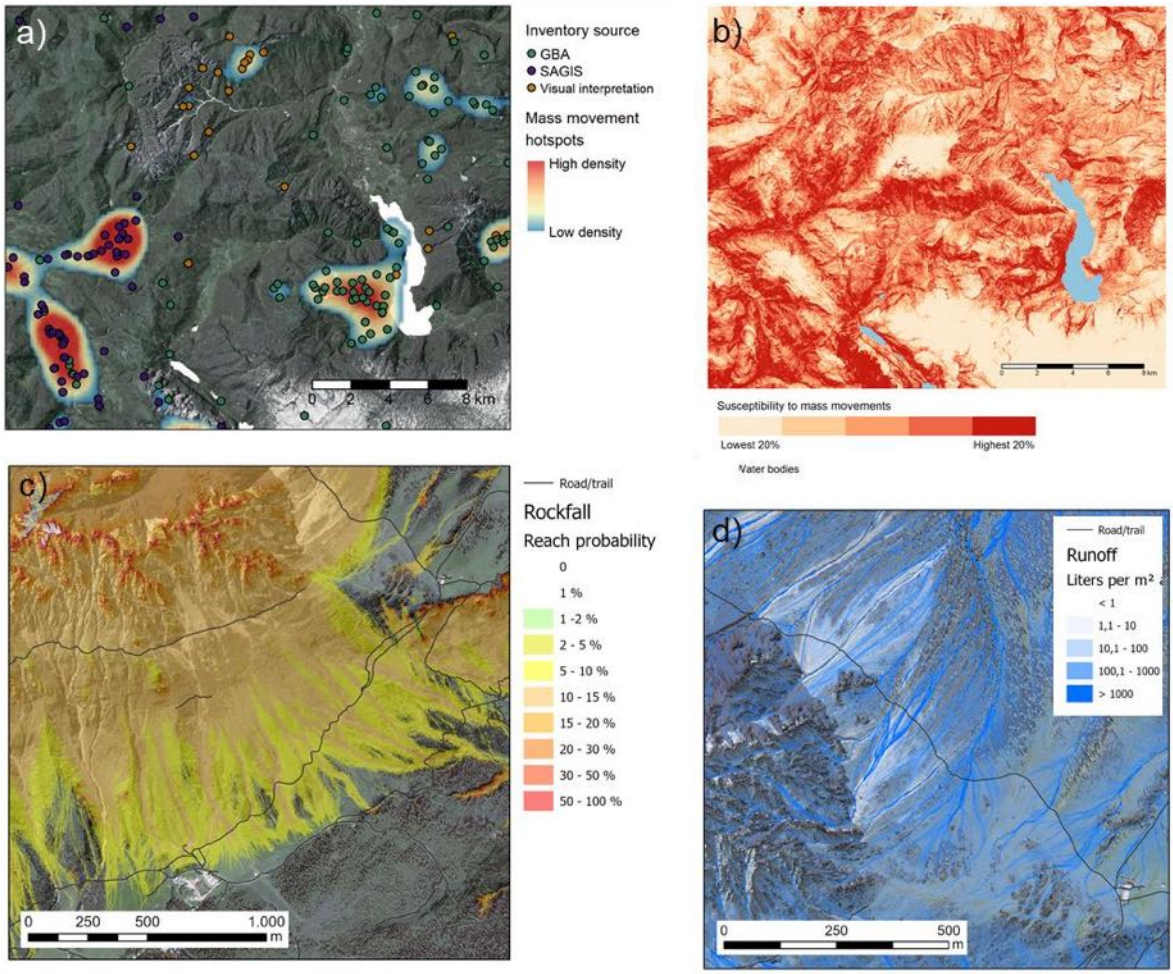

Figure 4: Digital maps about mass movements and erosion modelled from EO-derived information, digital elevation models (DEMs) and ancillary geodata, including a) mass movement hotspots, b) mass movement susceptibility, c) rockfall reach probability, and d) runoff-related erosion activity.

The derived information was overlaid on the trail network for each study area. Figure 5a shows susceptibility per trail segment and per alpine hut. Figure 5b shows rockfall reach probability per trail location. Figure 5c shows suggestions of alternative routes for trail relocation that avoid areas with strong mass movement activity.

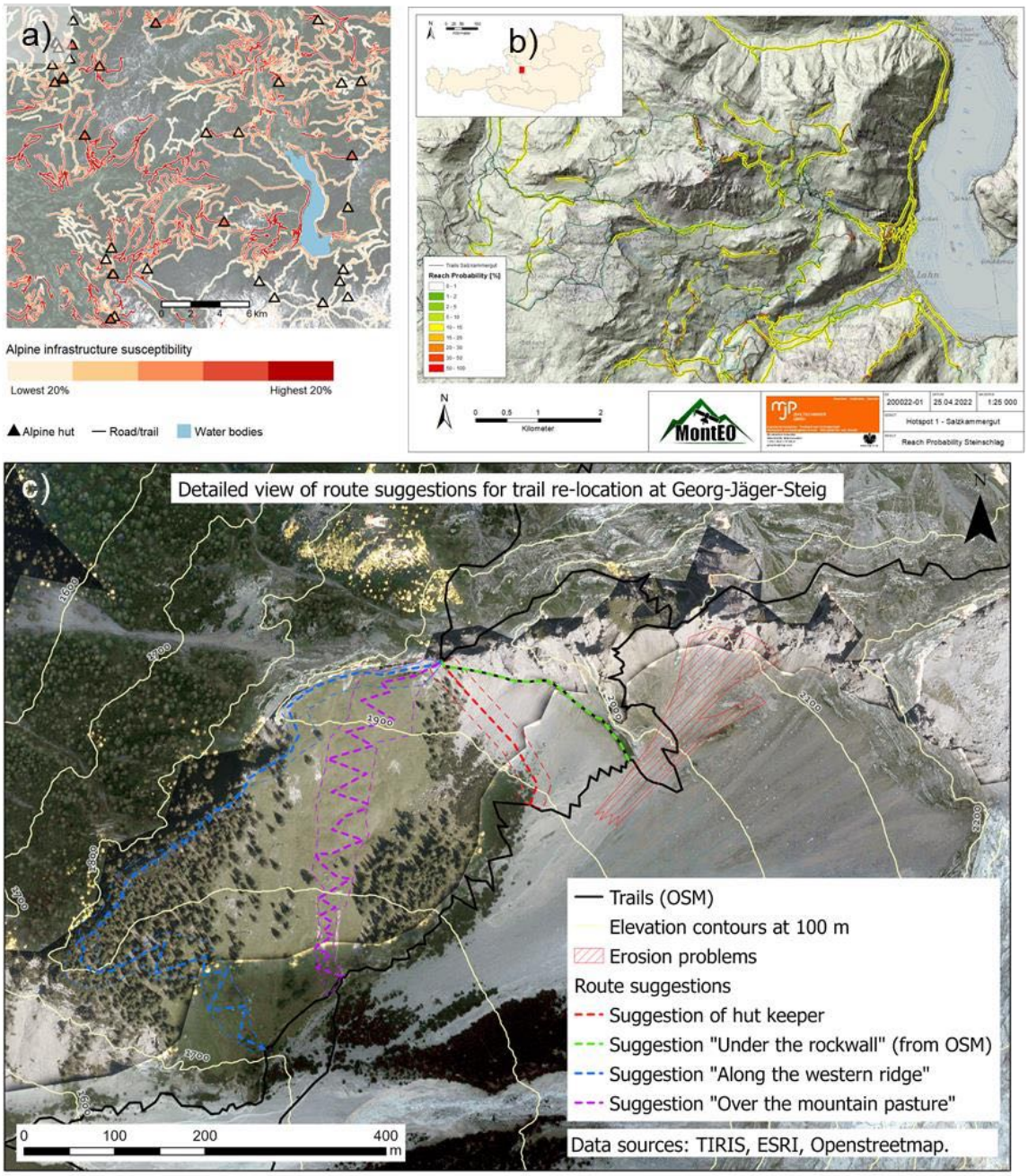

Figure 5: Digital Maps about mass movement impact on alpine infrastructure, including a) alpine infrastructure susceptibility, b) rockfall reach probability at trail locations, c) route alternatives for planning a trail relocation.

Discussion and Conclusion

The feedback from practitioners in trail keeping during the online questionnaire survey and the validation workshop confirmed the usefulness of the presented maps for the envisioned application cases. In particular, the susceptibility map provides well-targeted information for strategic effort planning. Positive elements include the comprehensive modelling approach that relies on a wide range of information. Furthermore, the cartographic visualisation emphasises the susceptibility at the alpine infrastructure elements, displays it with a well-suited legend, and allows to make an intercomparison for defining focus areas for alpine infrastructure management. A subject of debate was whether the information along the trails should be aggregated per trail segment or whether the map should display

susceptibility at the modelled resolution. Furthermore, the trail relocation map was rated as very useful for alpine infrastructure project planning. To achieve its full potential, the map should exclude any suggested route alternatives and include locally relevant information on mass movements and erosion provided with the other maps. Thereby, it can become the basis for guiding the discussion of local experts and stakeholders for a well-informed decision on the most suitable route for a new trail. In general, the trail keepers pointed out that the applicability and reliability of the maps need to be ensured by on-site verification.

The opportunities for advancing the development of the maps include methodological improvements and the adaptation of the maps to newly mentioned application cases, e.g., the use of the susceptibility map to justify an increase in funding provided by authorities or the use of rockfall models to support expert assessments with objective information. While further developments in close collaboration with users are needed, it has become apparent that EO data can provide information on the impact of mass movements on alpine infrastructure that is relevant for alpine associations. The project showed the potential of EO methods for use in alpine infrastructure management and identified key paths for their exploitation in practice.

Acknowledgements

This research has been supported by the Austrian Research Promotion Agency (FFG) in the Austrian Space Applications Program (ASAP) through the project MontEO (contract no: 873667). We would like to thank H. C. Dias from the University of São Paulo for her support in susceptibility modelling and discussion. Furthermore, we would like to thank G. Scheierl and T. Hipp from the German Alpine Association (DAV) and H. Resch, G. Resch and M. Platzer from the Austrian Tourist Club (ÖTK) for their valuable input and discussions. We also would like to thank the trail keepers from DAV, ÖTK and the Austrian Alpine Association (ÖAV) that participated in interviews and in the validation workshop for their valuable feedback.

References

Abad, L., Hölbling, D., Albrecht, F., Dias, H.C., Dabiri, Z., Reischenböck, G., Tešić, D., 2022. Mass movement susceptibility assessment of alpine infrastructure in the Salzkammergut area, Austria. *International Journal of Disaster Risk Reduction*, 103009.

Albrecht, F., Hölbling, D., Abad, L., Dabiri, Z., Reischenböck, G., Scheierl, G., Hipp, T., Resch, H., Resch, G., 2020. Mass movements documentation with EO data for assessing the impact on the alpine trails and huts infrastructure. *Disaster Research Days 2020 – Book of Abstracts*, pp. 200-203.

Albrecht, F., Hölbling, D., Weinke, E., Eisank, C., 2016. User requirements for an Earth observation (EO)-based landslide information web service. In: Aversa, S., Cascini, L., Picarelli, L., Scavia, C., eds. *Landslides and engineered slopes: experience, theory and practice*. CRC Press, 301-308.

Crosetto, M., Monserrat, O., Cuevas-González, M., Devanthéry, N., Crippa, B., 2016. Persistent scatterer interferometry: A review. *ISPRS Journal of Photogrammetry and Remote Sensing*, 115, 78-89.

Jones, J. N., Stokes, M., Boulton, S. J., Bennett, G. L., Whitworth, M. R. Z. (2020). Coseismic and monsoon-triggered landslide impacts on remote trekking infrastructure, Langtang Valley, Nepal. *Quarterly Journal of Engineering Geology and Hydrogeology*, 53(2), 159–166.

Mateos, R. M., García-Moreno, I., Reichenbach, P., Herrera, G., Sarro, R., Rius, J., Aguiló, R., Fiorucci, F. 2016. Calibration and validation of rockfall modelling at regional scale: application along a roadway in Mallorca (Spain) and organization of its management. *Landslides*, 13(4): 751-763.

Raso, E., Cevasco, A., Di Martire, D., Pepe, G., Scarpellini, P., Calcaterra, D., & Firpo, M. (2019). Landslide-inventory of the Cinque Terre National Park (Italy) and quantitative interaction with the trail network. *Journal of Maps*, 15(2), 818–830.

Back to table of contents

Tightly coupled GPS/IMU data integration for the estimation of vehicle trajectories

Qing Li, Robert Weber
Department of Geodesy and Geoinformation, TU Wien, Vienna, Austria

Abstract— Over the past years a software package employing the tightly coupled Kalman filter algorithm has been developed at the Department of Geodesy and Geoinformation (TU-Vienna). The software allows for the fusion of GPS and IMU data and accepts also odometer measurements, which enables a reliable vehicle positioning performance in post-processing mode. This approach has been utilized to estimate the trajectories of slow and fast-moving vehicles like cars or trains. A passenger vehicle or a rail vehicle can simply be equipped with a GPS unit, an IMU device, and other navigation sensors. Different GPS processing strategies based on the double-difference approach (DD) with code-only processing and combined code plus carrier phase processing are implemented and investigated. In the presented test cases, an iMAR IMU device and a JAVAD GPS receiver fixed on a private car provide the data input for the filter algorithm. The quality of our solution was assessed against trajectories calculated with the commercial Inertial Explorer software from NovAtel [Novatel]. All sensor data and reference trajectories were generated and provided thankfully by colleagues from the research group Navigation at TU Graz.

Keywords—Positioning, Kalman filter, Sensor fusion

I. INTRODUCTION

The vehicle positioning based on GPS and IMU integration to determine a precise and continuous trajectory of the moving vehicle has been investigated over several years in detail by various researchers. This technique is a non-contact, fast and accurate positioning method that has considerable potential for rail track or on-road positioning. Classically, a passenger car, a rail-mounted vehicle like a train, a ship, a plane, or a drone can be defined as vehicles (either manned or unmanned).

The integration of GPS and IMU sensor data delivers a mixture of position fixing and dead reckoning, which can be successfully employed for geodetic applications. The GPS provides a long-term, accurate absolute positioning solution at a lower measurement update rate (< 10 Hz) and independent of gravity. The main disadvantage of GPS standalone processing is the relatively low data rate, which causes problems in high kinematic applications. Furthermore, GPS must face its weak points, like blockage of line-of-sight signals, multipath and also signal interference or jamming. IMU standalone solutions are appropriate for short-term positioning and can provide a relative navigation solution at a high measurement update rate (up to 2000 Hz). Due to biases in the gyros and accelerometer measurements, sole IMU based trajectories suffer from significant sensor drifts. The quality of IMU standalone solutions degrades with time, and the accuracy depends on the quality of IMU sensor. The sensor fusion can limit IMU drift errors by GPS update information. On the other hand the IMU cannot be jammed and can help to detect GPS carrier phase cycle slips and supports a precise tracking of the Doppler shift. Therefore, the advantages of an integrated system are more than just an improvement of positioning accuracy. By sensor fusion, the advantages of each sensor can compensate for drawbacks of the other.

Kalman filter-based estimation was invented by Prof.R.E.Kalman in 1960 [Groves, 2013]. This technique constitutes an optimum stochastic approach for parameter estimation and is commonly used for processing real-time sensor data and in data fusion. This research aims to develop software capable of performing the states of a land vehicle trajectory by exploiting a tightly coupled Kalman filter scheme. One basic code-only and one combined code-phase GPS/IMU integration scheme were set up. As input, the IMU measurements and the raw GPS measurements of the rover- and reference-station can be imported and processed. In the GPS data processing, the ionosphere-free linear combination (dual frequency observations) is used to remove the influence of the ionosphere. The IMU navigation equations are implemented in the local level frame with NED coordinate directions. This frame allows for an easy visualization of the navigation solution.

Overall, three data sets gathered by an motor vehicle on test drives on the same route with their respective reference trajectories are obtained for quality testing of the software. The reference trajectories were obtained from data processing utilizing the commercial software Inertial Explorer from the Waypoint Company. A dual-frequency geodetic-grade receiver (JAVAD) and a strapdown IMU device from the company iMAR Navigation were rigidly equipped on a stable platform on the roof of the car. The GNSS reference station data was obtained from an EPOSA station located on the roof of Graz main train station. Due to the fast movement of our rover, the DD carrier phase ambiguities are estimated as float biases instead of fixed to integers. Of course, this fact somehow limits the positioning accuracy to dm-level instead of cm-level.

After considering the theoretical background in chapter 2 the structure of our filter scheme is described in chapter 3. Chapter 4 introduces the involved sensor equipment and discusses the observations fed to the filter. Chapters 5 and 6 describe the field test settings. Finally, chapter 7 focuses on the test drive results which are compared to the reference trajectories in order to analyze the quality of the software

II. KALMAN FILTER FOR GPS/IMU INTEGRATION

Concerning the GPS data our algorithm utilizes DD combined code plus phase observations. The implemented state vector consists of the following 15 state components + phase biases of the visible satellites:

$$\delta x^n = (\delta r^n, \delta v^n, \delta \psi^n, b_a, b_g, phase\ biases) \quad (1)$$

where δr^n is the position error that may be expressed in a n-frame as the geodetic coordinates δφ, δλ and δh. δv^n is the velocity error which may be expressed in $\delta V_E, \delta V_N, \delta V_D$ components. $\delta \psi^n$ describes the attitude angles of the vehicle. Accelerometer biases *ba,* gyroscope biases *bg*, and the phase biases to all visible satellites complement the state vector. In our approach initial values of the phase biases are calculated by a LSQ scheme and then fed to filter which definitely reduces convergence times.

In general, the Kalman filter algorithm comprises three main steps: calculation of the Kalman gain, prediction, and update. We use a prediction equation of the state vector x to describe the dynamic system model as:

$$\dot{x}_k = F_{(k,k-1)}\, x_{(k,k-1)} \quad (2)$$

where $\dot{x}_k$ is the linear function of x, $F_{(k,k-1)}$ is the system dynamics matrix. k denotes the current epoch. We can define the propagation of the state vector with respect to time by means of:

$$\hat{x}_k = \Phi_{(k,k-1)}\hat{x}_{(k,k-1)} \quad (3)$$

where $\Phi_{(k,k-1)}$ is the transition matrix. The hat operator "$\hat{x}_k$"denotes a Kalman filter estimate of the state vector. The relationship between $F_{(k,k-1)}$ and $\Phi_{(k,k-1)}$ reads as:

$$\Phi_{(k,k-1)} = \exp(F_{(k,k-1)}\, dt) \quad (4)$$

The error covariance propagation can be formulated by:

$$P_k = \Phi_{(k-1)} P_{(k-1)} \Phi^T_{(k-1)} + Q_{(k-1)} \quad (5)$$

where $P_k$is the error covariance matrix, Q_k is the system noise covariance matrix. The IMU state error (symbol "δ") is simply the difference between the raw IMU measurement solution (symbol "~") and the corrected inertial navigation solution (symbol "^"). This relationship in terms of position and velocity can be described as follows [Groves, 2013]:

$$\hat{r}^n = \tilde{r}^n - \delta r^n, \hat{v}^n = \tilde{v}^n - \delta v^n \quad (6)$$

In terms of attitude the IMU state error can be expressed in form of the coordinate transformation matrix from the b-frame to n-frame, C_b^n:

$$\hat{C}_b^n = (I - E^n)\tilde{C}_b^n \quad (7)$$

Here the skew symmetric matrix E^n, with the components resolved in the NED axes, is used to describe the attitude error:

$$E^n = (\epsilon^n \times) = \begin{pmatrix} 0 & -\epsilon_D & \epsilon_E \\ \epsilon_D & 0 & -\epsilon_N \\ -\epsilon_E & \epsilon_N & 0 \end{pmatrix} \quad (8)$$

The IMU position error propagation is dependent on the position and velocity of the vehicle. Building the partial derivatives of the position and velocity difference vectors, the IMU position error propagation for a n-frame can be formulated as [Blauensteiner, 2008]:

$$\delta \dot{r}^e = F_{rr}\delta r^e + F_{rv}\delta v^n \tag{9}$$

The IMU velocity error propagation can be formulated as:

$$\delta \dot{v}^n = F_{vr}\delta r^e + F_{vv}\delta v^n + \epsilon^n \times f_{ib}^n + C_b^n \delta f_{ib}^n + \delta g^n \tag{10}$$

Finally, the attitude error propagation is described by:

$$\dot{\epsilon}^n = F_{er}\delta r^e + F_{ev}\delta v^n - w_{in}^n \times \epsilon^n - C_b^n \delta w_{ib}^b \tag{11}$$

w_{in}^n can be obtained from

$$w_{in}^n = \begin{pmatrix} w_e cos\varphi + V_E/(N+h) \\ -V_N/(M+h) \\ -w_e sin\varphi + V_E tan\varphi/(N+h) \end{pmatrix} \tag{12}$$

where w_e = 7.2821158 rad/s stands for the rotation rate of the Earth [Shin, 2001]. We also consider the residual biases, *ba* and *bg*, of our acceleration and gyro sensors:

$$\delta f_{ib}^b = b_a, \delta w_{ib}^b = b_g \tag{13}$$

We assume that the biases are stable in time. Therefore, their variations can be fixed to zero [Groves, 2013].

$$\dot{b}_a = 0, \dot{b}_g = 0 \tag{14}$$

The system dynamics matrix can be defined as:

$$F = \begin{pmatrix} F_{rr} & F_{rv} & 0 & 0 & 0 \\ F_{vr} & F_{vv} & (f^n \times) & C_b^n & 0 \\ F_{er} & F_{ev} & -(w_{in}^n \times) & 0 & C_b^n \\ 0 & 0 & 0 & 0 & 0 \\ 0 & 0 & 0 & 0 & 0 \end{pmatrix} \tag{15}$$

The update processing starts from the following observation equation:

$$\delta z_k = z_k - H_k \hat{x}_k \tag{16}$$

where z_k denotes the measurement vector at epoch k. H is the design matrix. H and z together make up the measurement model based on the observation differences between GPS and IMU.

In a tightly coupled approach the GPS observations, (code and phase pseudo-ranges, carrier-phase and pseudo-range rate observables, and doppler shift tracking) are used for the measurement update. The difference between the GPS pseudo-range observations and the corresponding predicted IMU pseudo-range and pseudo-range rate quantities constitute the Kalman filter innovation. Therefore, the measurement vector comprises the combined code and carrier-phase pseudo-range differences as well as the range-rate differences between both sensors for m satellites tracked.

$$z_k = \begin{pmatrix} \delta z_{\rho,k} \\ \delta z_{\phi,k} \\ \delta z_{r,k} \end{pmatrix} \tag{17}$$

where

$$\delta z_{\rho,k} = \left[\rho_{r,gps}^p - \rho_{m,gps}^p\right] - \left[\rho_{r,gps}^s - \rho_{m,gps}^s\right] - \left[\rho_{r,imu}^p - \rho_{m,imu}^p\right] - \left[\rho_{r,imu}^s - \rho_{m,imu}^s\right]$$

,

$$\delta z_{\rho,k} = \left[\lambda\phi_{r,gps}^p - \lambda\phi_{m,gps}^p\right] - \left[\lambda\phi_{r,gps}^s - \lambda\phi_{m,gps}^s\right] + \lambda N_{r,m}^{s,p} - \left[\rho_{r,imu}^p - \rho_{m,imu}^p\right] - \left[\rho_{r,imu}^s - \rho_{m,imu}^s\right]$$

and

$$\delta z_{r,k} = \left[\dot{\rho}_{gps}^s - \dot{\rho}_{imu}^s\right] \tag{18}$$

where the GPS code pseudo-range and carrier phase $\rho_{r,gps}^s$ and $\phi_{r,gps}^s$ measurements are already corrected for atmospheric delays. p denotes the pivot satellite. The pseudo-range rate $\dot{\rho}_{gps}^s$ can be derived from the GPS doppler shift measurement. $\dot{\rho}_{imu}^s$ and $\rho_{m,imu}^s$ are the pseudo-range and pseudo-range rate derived from the IMU observations. Also the offset (lever arm) between GPS antenna and IMU device has to be accounted for when the IMU predictions are updated. $\lambda N_{r,m}^{s,p}$ is the phase bias attained by differencing the phase observations between the rover and the reference station.

We also define the H_k matrix, representing how the measurement vector, z_k, varies with the state vector. We must recalculate the matrix on each iteration. In the GPS/IMU integrated system, the H_k matrix is a function of the user dynamics, which bases on the combined code and carrier phase approach. For the n-frame H_k is defined by:

$$H_k^n = [H_{k,1}^n, H_{k,2}^n] \tag{19}$$

where

$$H_{k,1}^n = \begin{pmatrix} h_L u_{a1,N}^n & h_\phi u_{a1,E}^n & u_{a1,D}^n & 0 & 0 & 0 & 0 & 0 & 0 \\ h_L u_{a2,N}^n & h_\phi u_{a2,E}^n & u_{a2,D}^n & 0 & 0 & 0 & 0 & 0 & 0 \\ \vdots & \vdots & \vdots & \vdots & \vdots & \vdots & \vdots & \vdots & \vdots \\ h_L u_{am,N}^n & h_\phi u_{am,E}^n & u_{am,D}^n & 0 & 0 & 0 & 0 & 0 & 0 \\ 0 & 0 & 0 & h_L u_{a1,N}^n & h_\phi u_{a1,E}^n & u_{a1,D}^n & 0 & 0 & 0 \\ 0 & 0 & 0 & h_L u_{a2,N}^n & h_\phi u_{a2,E}^n & u_{a2,D}^n & 0 & 0 & 0 \\ \vdots & \vdots & \vdots & \vdots & \vdots & \vdots & \vdots & \vdots & \vdots \\ 0 & 0 & 0 & h_L u_{am,N}^n & h_\phi u_{am,E}^n & u_{am,D}^n & 0 & 0 & 0 \\ 0 & 0 & 0 & 0 & 0 & 0 & -u_{a1,N}^n & -u_{a1,E}^n & -u_{a1,D}^n \\ 0 & 0 & 0 & 0 & 0 & 0 & -u_{a2,N}^n & -u_{a2,E}^n & -u_{a2,D}^n \\ \vdots & \vdots & \vdots & \vdots & \vdots & \vdots & \vdots & \vdots & \vdots \\ 0 & 0 & 0 & 0 & 0 & 0 & -u_{am,N}^n & -u_{am,E}^n & -u_{am,D}^n \end{pmatrix} \tag{20}$$

and

$$H_{k,2}^n = \begin{pmatrix} 0 & \cdots & 0 & \cdots & 0 & 0 & 0 & 0 \\ 0 & \vdots & 0 & 0 & 0 & 0 & 0 & 0 \\ 0 & 0 & 0 & 0 & 0 & 0 & \vdots & \vdots \\ 0 & 0 & 0 & 0 & 0 & 0 & 0 & 0 \\ -\lambda & 0 & 0 & 0 & 0 & 0 & 0 & 0 \\ 0 & 0 & 0 & -\lambda & 0 & 0 & 0 & 0 \\ 0 & 0 & 0 & 0 & \vdots & 0 & \vdots & \vdots \\ 0 & 0 & 0 & 0 & 0 & -\lambda & 0 & 0 \\ 0 & 0 & 0 & 0 & 0 & 0 & 0 & 0 \\ 0 & 0 & 0 & 0 & 0 & 0 & 0 & 0 \\ 0 & \vdots & \vdots & \vdots & \vdots & \vdots & -\lambda & \vdots \\ 0 & \cdots & 0 & \cdots & 0 & \cdots & 0 & 0 \end{pmatrix} \tag{21}$$

where

$$h_L = -(M+h), h_\phi = -(N+h)cos\phi \tag{22}$$

M is the radius of curvature along the meridian, and N is the radius of curvature along the parallel of latitude. u^n is the line of sight vector, which defines the direction from the user antenna to the satellite. In the n-frame u^n is formulated as:

$$u^n = C_e^n \frac{r^{e,s} - r_r^e}{|r^{e,s} - r_r^e|}, u^n = (u_N^n, u_E^n, u_D^n) \tag{23}$$

An important element of the Kalman filter is the Kalman gain, K_k. This matrix represents the weighting between measurement and the observable gained from the state vector. The Kalman gain calculation can be performed as follows:

$$K_k = P_k H_k^T (H P_k H_k^T + R_k)^{-1} \tag{24}$$

where R_k is the measurement noise covariance matrix, P_k is the error covariance matrix. The measurement noise is environmentally dependent, but also elevation-angle-dependent. Therefore we apply an apriori elevation dependent weighting and the measurement noise components can be described as follows:

$$\sigma_\rho = \frac{\sigma_{code}^2}{sin^2(el)}, \sigma_\phi = \frac{\sigma_{phase}^2}{sin^2(el)}, \sigma_{\dot{\rho}} = \frac{\sigma_{doppler}^2}{sin^2(el)} \tag{25}$$

By means of the measurement vector and the Kalman Gain matrix the update of the state vector can be formulated as follows:

$$\hat{x}_k = \hat{x}_{\bar{k}} + K_k(z_k - H_k \hat{x}_{\bar{k}}) \tag{26}$$

III. STRUCTURE OF A TIGHTLY COUPLED KALMAN FILTER

The structure of our tightly coupled algorithm is designed in figure 1.

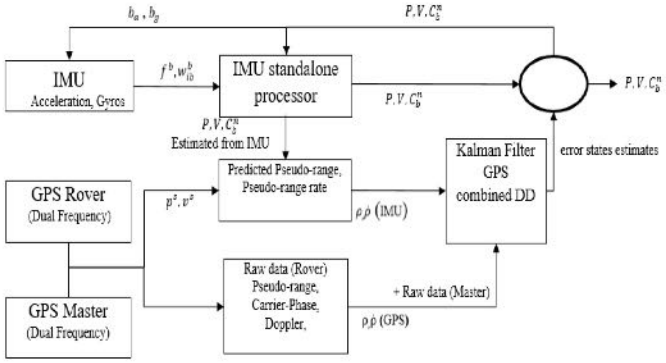

Figure 1: Structure of a tightly coupled Kalman filter based on GPS DD observations

Once raw GPS data of the rover and the reference station have been acquired, the Kalman filter algorithm has to be initialized. For the initialization, satellites with an elevation angle above 5° visible for both the rover and the reference station are selected. To speed up convergence of the KF later on, the initial position and velocity of the rover, initial float ambiguity values and their error covariance are estimated using an least-squares adjustment by processing GPS DD code plus phase data over a few epochs. The iterative part of the GPS/IMU integration algorithm starts after reading the IMU measurements. The IMU data contains the accelerations and angular rate observations in the x, y and z directions recorded in GPS-time. By applying the lever-arm vector between the GPS antenna and the IMU device also the initial position of the IMU device is determined. The developed tightly Kalman filter directly uses the difference between the measured GPS raw observations and corresponding 'pseudo-observations' derived from the IMU data. These differences are fed back into the navigation solution of the IMU and allow correcting also for sensor biases.

IV. TEST DRIVE-DEVICES

The test drive was carried out in the area of Graz with a private car. The car has been equipped with a GNSS antenna and dual-frequency, dual-system receiver from the JAVAD Company. In addition an IMU device of the iMar company has been mounted on the car's roof. An EPOSA station located permanently on the roof of the Graz main train station was chosen as the GNSS reference station. The data sets are composed of about 1 hour of recorded sensor measurements, which contain static and kinematic parts. The test drive covers more than 11 km driving distance. The reference station is located within 12 km of all rover's points along the test route, and delivers reference observables at 1 Hz update rate.

Each test drive data set contains the raw GPS measurements (o.file and n.file) from rover and reference station, as well as the corresponding IMU measurements. The employed IMU device is a strapdown high accurate navigation-grade device from the iMar family type iNAV-RQH-003. The device carries three servo-accelerometers type QA2000-40 (Q-Flex) and three high precision laser gyroscopes type GG1320. This device is characterized by improved performance parameters, such as bias and scale factor stability, linearity, and acceleration sensitivity. Table 1 gives you an overview of the most important specifications of this IMU device.

iNAV-RQH-003		
	Gyroskope performance Ramdom walk Drift	 < 0.0025° /$\sqrt{h}$ < 0.003°/hr
	Accelerometer performance Ramdom walk Bias	 < 8μ$\sqrt{Hz}$ < 100 μg
	Data Rate Price of the sensor	2000 Hz 160.000 Euro

Table 1: The specification of the device [iMar]

This IMU device is mounted on the tailored calibrated platform on the private car's roof. At the same time, the GPS antenna and receiver has been mounted at this platform for the simultaneous measurement of the sensors (figure 2 and figure 3). The IMU device output has been synchronized to GPS-time, which is an indispensable precondition for sensor fusion.

Figure 2: GNSS and IMU sensors mounted on the private car's roof [laengauer,2010]

A surveying company measured the lever-arm vector between the GPS antenna and IMU device. The finally applied lever-arm between the IMU device to GPS antennas amounts to: [-0.001m, 1.097m, 0.153m].

Figure 3: tailored calibrated platform applied for the sensor fusion [Wieser, 2019]

This IMU-device recorded and provided data from the accelerometers and gyroscopes with the highest available data rate of 2000 Hz.

Figure 4: The relationship between the IMU axes and the vehicle axes [TU Graz, 2019]

In general, the IMU provides its measurement in the body frame. The n-frame is defined using an East-North-Up (ENU) coordinate system or an East-North-Down (NED) coordinate system. The iNAV-RQH family outputs for land vehicles (e.g., a car or a train), always refer to an ENU as the n-frame. On the

other hand, for the aircraft and watercraft [iMar], the IMU output always refers to an END as the n-frame. In this research, the n-frame of the final navigation solution was defined as a NED-frame. Thus, a coordinate transformation had to be carried out to transform the measured IMU data based on ENU system to the NED.

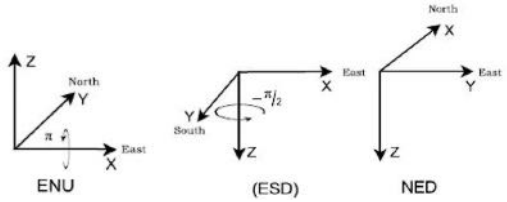

Figure 5: The transformation from ENU to NED consists of two rotations in Roll and Yaw directions (from left side to right side) [GRANDIN, 2007]

The transformation matrix between both systems can be formulated as follows [Grewal, 2006]:

$$C_{NED}^{ENU} = \begin{pmatrix} 0 & 1 & 0 \\ 1 & 0 & 0 \\ 0 & 0 & -1 \end{pmatrix} \tag{27}$$

The GNSS data sets used as the rover for the first drive test were recorded by a geodetic dual-frequency GPS/GLONASS receiver from Javad type Sigma TRE-G3TH with a Javad GrAnt-G3T antenna. This receiver is capable of receiving L1, L2, and L5 GPS signals [Laengauer, 2010].

Figure 6: Javad GrAnt antenna (left) and Javad Sigma TRE-G3TH receiver (right) [GlobalPOS]

We set the logging data rate of the GPS receiver to 5 Hz during the test drive.

V. SOFTWARE SETTINGS

Table 2 shows an overview of the parameter settings within the TU software to process data of the test drive. The software uses the ionosphere-free combination to process dual-frequency data to eliminate the ionospheric delay and applies the Vienna Mapping Function 3 (VMF3) or the Saastamoinen model to eliminate the tropospheric delay. The software also considers error corrections in SPP mode such as phase wind-up, solid earth tides, relativistic corrections, etc.

iNAV-RQH-003	
Station	Rover + reference station
Device	GPS & IMU
GPS observation	Single point positioning (PPP code-only) DD code-only, DD combined code+ phase
Processing mode	Post-processing, kinematic
Date rate	IMU: 2000 Hz GPS: 5Hz
Integration frequency	200 Hz
Observation weighting model	Satellite elevation $(\sin(el)^2)$
STD GPS raw observation	Code: 20 cm Phase: 0.8 cm Doppler: 20cm
Cut-off angle	Elevation 5 °
Satellite orbit and clock correction	GFZ final product for the PPP processing
Satellite and receiver antenna	IGS Antex igs14.atx
Troposphere model	VMF3, Saastamoinen model
Ionosphere model	Ionosphere-free linear combination (L1,L2)
Phase ambiguity	Float solution
Cycle Slip detection	Doppler measurement based
Other correction model	Phase wind-up, solid earth tides, relativistic correction and sagnac effect
Min. number of satellite	2

Table 2: General processing settings used for the tightly coupled GPS/IMU integration

VI. TRACK OF TEST DRIVE

Data was recorded on May, 19th, 2019, starting at 10:13h (UTC). Firstly, we analyze the estimated yaw angles to match these with the route traveled by car (figure 7).

The starting point and the end of the test drive is visible on the left side of figure 7, where the car stopped on a parking lot for at least 10 minutes. The vehicle was placed at a location about 11km away from the reference station in Graz. Later, the car drove along the roundabout and finally getting back to the parking lot.

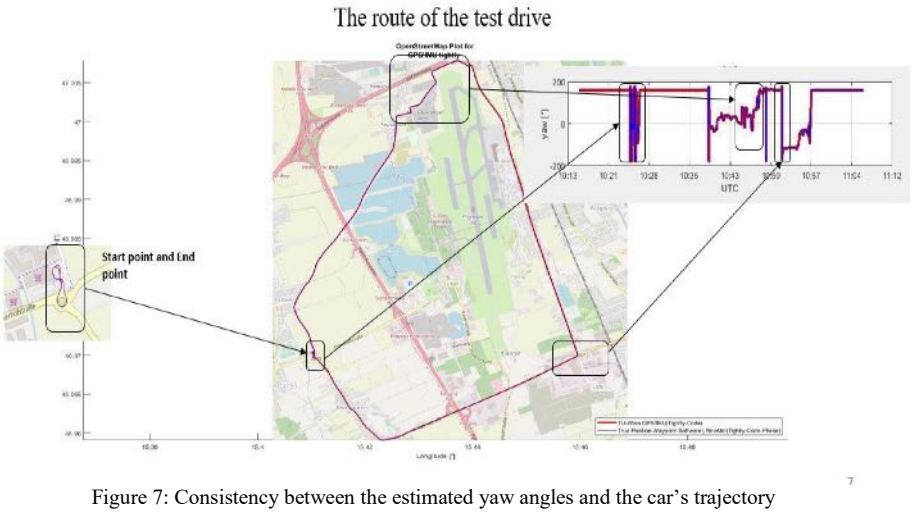

Figure 7: Consistency between the estimated yaw angles and the car's trajectory

A first short drive took about 2 minutes, afterwards the car has stopped for about 15 minutes. At 10:42, the car started again moving in the north direction to the Graz airport. After passing the airport the vehicle moved back in the south direction to the starting point. Thus the test drive was simply a 25 minutes ride around the Graz airport. At about 11:10 (UTC) the sensors were turned off and the data logging stopped. Figure 7 shows the two-dimensional horizontal trajectories of the vehicle estimated by both the reference software and TU software. The trajectories were represented in the Open street map. The blue line denotes the estimated horizontal coordinates employing the Waypoint software, and the red line represents the estimated vehicle trajectory using the TU software. However, as both lines overlap all the time, the coordinate differences cannot be shown clearly at this scale. The differences in position between both software solutions are just in the few dm range.

VII. TEST DRIVE-RESULTS

In the following, we look more detailed at the results obtained with the TU-developed GPS/IMU integration algorithm. Our software allows to select between three modes for GPS data processing, namely a) DD Phase+Code observations, b) DD Code observations and c) just a zero-difference code solution (SPP). Here the chosen approach is consistent with the approach used by the reference software: combining the DD combined code and carrier phase observations and IMU measurements at the raw data level. The only difference is that the reference software processes GPS/GLONASS observations, while the TU solution is just based on GPS observations.

Figure 8 displays the three-dimensional position differences between the TU software solution compared to the reference solution. The differences in unit meters are plotted in North, East and Height directions.

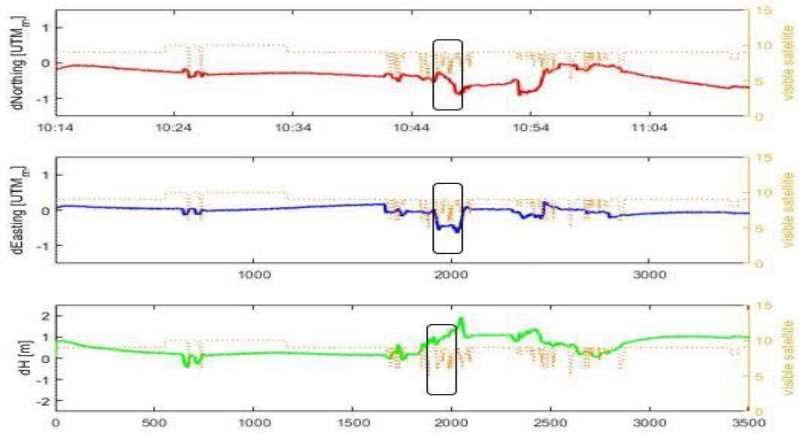

Figure 8: Positioning differences between solution from Waypoint Software and TU-Wien software

As already mentioned the differences in North and East components are relatively small at the few dm-level. In the height, the deviation is within a range of a few decimeters up to 1.5meter.

Due to the rover's movement and therefore varying signal blockings, the software has to account for permanent changes in visible satellites. A problem, especially evident, when the reference satellite has to be switched. Our software requires that the elevation of a new reference satellite has to be at least 1 degree higher than the elevation of the current one.

At 10:46, we lost the signal of the reference satellites several times for short periods. Each signal loss causes a switch to new reference satellites and subsequently requires that all ambiguities are reinitialized and to be referred to the new reference. This problem makes the results at these epochs worse and more unstable, clearly seen in Figure 8. Another problem occurs at 10:42. There is a big jump of all visible satellites in the carrier-phase measurement of the reference station at this epoch. The implemented cycle slip detector could identify these jumps at the current epoch, and the software reinitialized the ambiguity for all satellites to fix this problem automatically.

Furthermore, the golden line represents the number of visible satellites. It should also be noted: if the number of visible satellites is changing, the deviations between both solutions are also changing simultaneously.

When the car was at rest, the deviations between both software solutions of course diminished and the results are more stable.

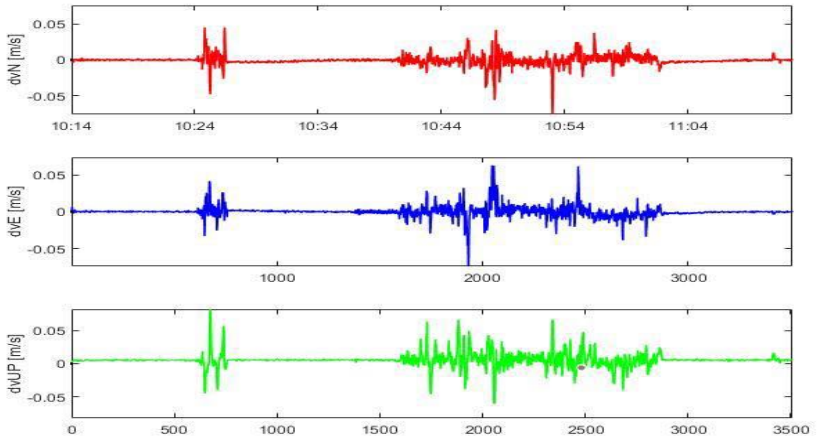

Figure 9: Velocity differences between solution from Waypoint Software and TU-Wien software

To assess the quality of the velocity components, the differences between both solutions are depicted in figure 9. The figure clearly shows that the deviations in all three directions are within a range of 0.05 m /s, when the car moves. When the car is at rest, the deviations are much smaller.

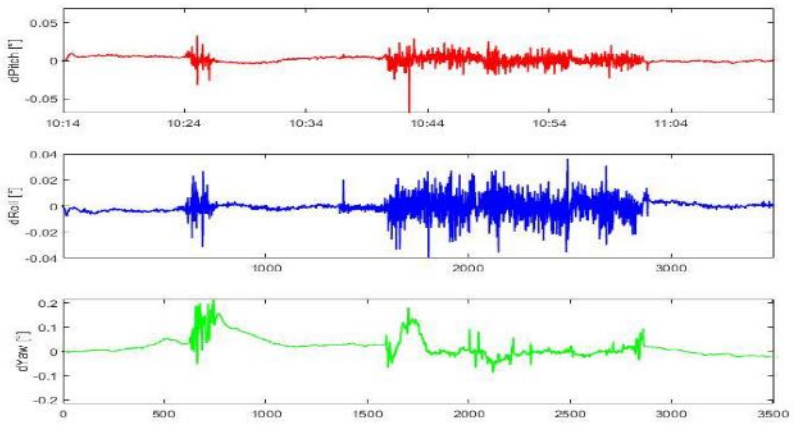

Figure 10: Pitch/Roll/Yaw differences from Waypoint Software and TU-Wien

Last, but not least, figure 10 shows pitch, roll and yaw angles differences estimated by means of the TU software and the reference software. While the car is in movement, deviations in roll and pitch angles within 0.05 degrees show up, while as expected the yaw angle estimates deviate within a range of 0.2 degrees.

As noted above, our software allows to select between three modes for GPS data processing. The GPS data was processed in all 3 modes and figures 11, 12 and 13 below display the difference time series of all approaches with respect to the reference solution. The red line always refers to the DD code+phase approach as discussed in figures 8-10. The blue line represents the difference between the TU solution based on the DD code-only processing algorithm compared with the reference solution. The green line shows the difference based on SPP.

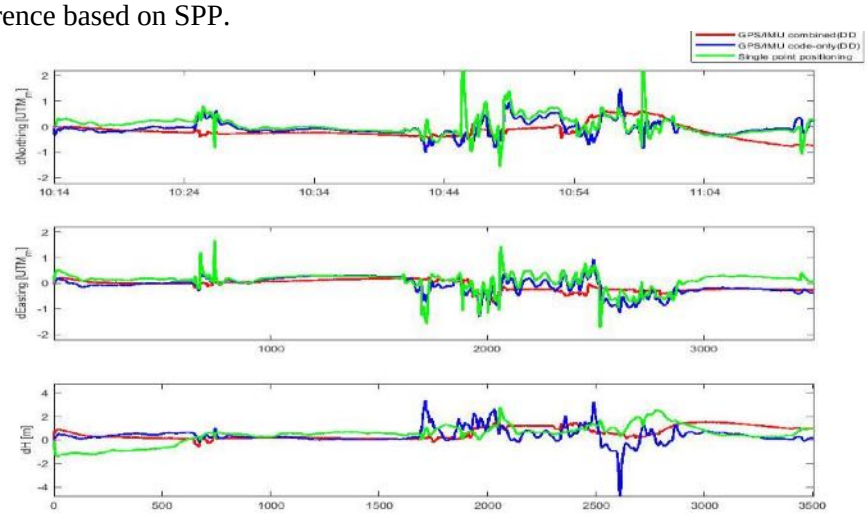

Figure 11: Position differences with respect to Waypoint reference solution (red: DD code+phase; blue: DD code only; green: code SPP)

As assumed, the differences between the TU solution based on the DD combined processing and the reference solution are smallest and most stable over the whole test drive. The SPP time series experience the most significant differences in the horizontal position (up to meter level), and interestingly the DD code-only approach indicates the biggest differences in the vertical.

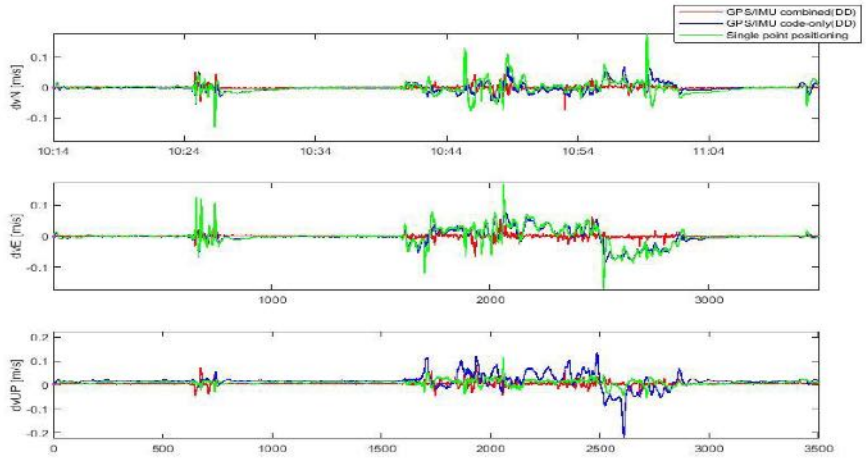

Figure 12: Velocity differences with respect to Waypoint reference solution (red: DD code+phase; blue: DD code only; green: code SPP)

Concerning the velocity components the DD code+phase approach delivers the best and most stable solution as expected. More noisy but with only slightly larger velocity differences the DD code solution performs better than expected in the plane coordinates. The SPP solution experiences peaks in the velocity differences up and slightly above 0.1 m/s.

In figure 12, the red line represents the slightest difference in the velocity solutions in all three directions. The blue line shows a better solution than the green line in the horizontal direction.

The line represents the worst velocity solution in the vertical direction.

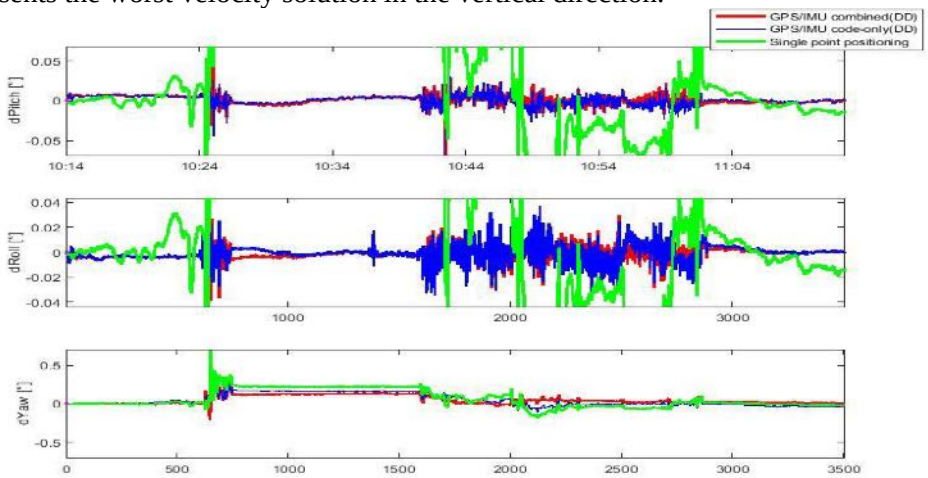

Figure 13: Differences in roll, pitch and yaw angles

The differences in the attitude angles are quite comparable for the DD code+phase and DD code-only solutions and are within 0.02 deg for roll and pitch and within 0.2 deg for the yaw angle. As expected, the SPP solution clearly performs worst as displayed in figures 13.

VIII. TEST DRIVE-THE CARRIER SMOOTHED CODE

We had to note that the previous results were based on already filtered GPS code ranges. The code observations were carrier-smoothed before entering the filter as the original raw code measurement is very noisy and unstable. The Carrier-smoothed-code algorithm for dual frequency measurement is expressed as follows [Sanz Subirana, 2011].

$$P(k)_r^s = \frac{1}{n}P(k)_r^s + \frac{n-1}{n}\left(P(k-1)_r^s + \lambda(L(k)_r^s - L(k-1)_r^s)\right) \quad (28)$$

where $P(k)_r^s$ and $L(k)_r^s$ are the code and carrier-phase measurements made by receiver r from the satellite s at epoch k. $P(k)_r^s$ denotes the smoothed code measurement in meter. n is the smoothing weight factor. The smoothed code measurement to the current time (k) bases on the estimated code measurement from

the previous epoch (k-1) and the difference of the carrier-phase measurements between the last epoch and the current epoch.

To show the effect of this smoothing the DD code-only solution was processed once with the raw code observations and once with the carrier smoothed code ranges.

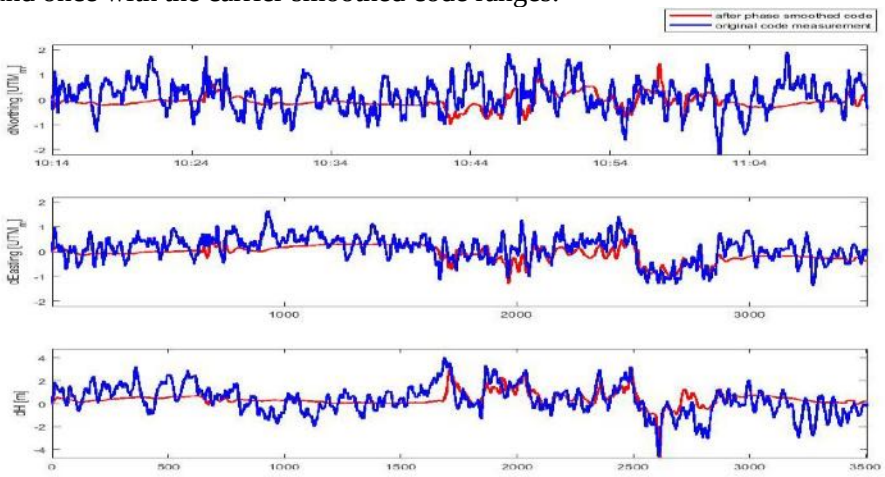

Figure 14: Position differences between solutions from Waypoint software and TU-Wien software. The blue line represents the solution difference calculated with the original GPS measurements, and the red line shows the solution differences after using phase smoothed code.

The smoothing effect is clearly visible in figures 14 and 15. The position noise decreases from meter to dm level. Also the velocity components show a clearly improved behavior.

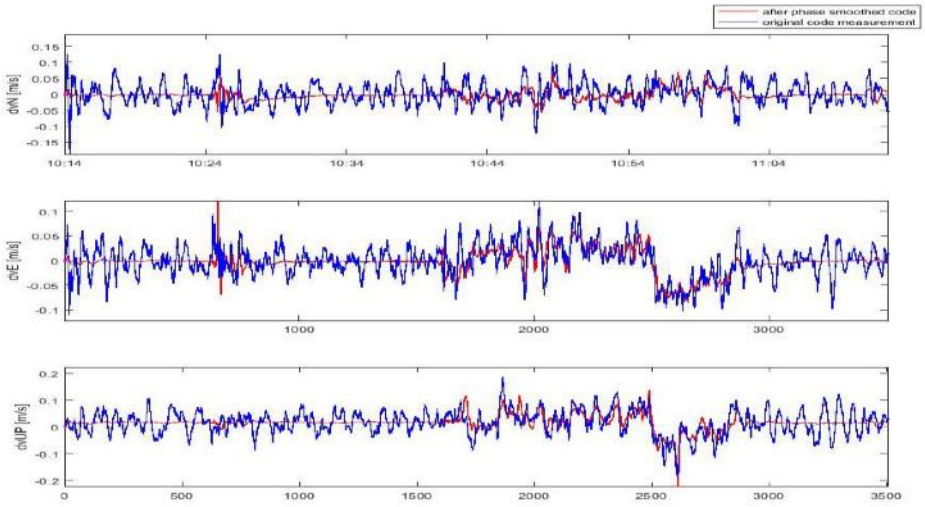

Figure 15: Velocity differences between Waypoint reference solution and TU-Wien DD code only solution based on raw code ranges (blue) and phase smoothed code ranges (red)

Figure 15 shows two differences in velocity solutions. There is also a clear improvement to see that velocity differences shown as the red line are smaller and more stable, which is based on using the phase smoothed code system.

IX. CONCLUSION

At TU-Vienna a software solution for tightly coupled GPS/IMU sensor integration has been successfully designed and implemented. The algorithm supports different GPS observation processing strategies based on DD phase and code observations but can handle also code-only scenarios.

In this research the trajectory of a moving car was processed by the in-house software and the results were compared with the reference solution calculated with the commercial Waypoint software. The position differences for the DD-code+phase approach in the plane coordinates are quite small at the few dm level while in height differences up to 1m show up. The differences in the velocity components and

attitude angles are at the 0,05m/s and 0.1 deg level. Also DD code and SPP scenarios were processed to evaluate the potential of cheap sensor data just offering phase-smoothed code ranges in combination with high quality IMU data.

In the future, we plan to augment our filter software solution also for processing odometer data. This augmentation would of course stabilize the state vector in periods of GPS signal blocking and shall be used for processing sensor data tracked at fast moving trains.

X. REFERENCE

1. Klemens Laengauer. "*Trajektorienbestimmung mittels Integration von GNSS und IMS*". Master's thesis. Technische Universität Graz, 9.2010.

2. Eugenio Realini. "*GoGPS-free and constrained relative kinematic positioning with low cost receivers*". PhD thesis. Politechnico di Milano, 2009.

3. Naser El-Sheimy. "*The Potential of partial IMU for land vehicle navigation*". Inside GNSS, Spring 2008, pp. 16-25

4. J. Sanz Subirana. "*Carrier-smoothing of code pseudoranges*". ESA Navipedia, TU Catalonia, Spain.2011.

5. Paul D.Groves. "*Principles of GNSS, Inertial, and Multisensor Integrated Navigation Systems, second Edition*". ISBN: 9781608070053, 2013

6. Jesper Grandin. "*Aided inertial navigation field tests using an RLG IMU*". Master's thesis, school of architecture and the built environment, KTH, Sweden, 2007

7. Mohinder S. Grewal. "*Global Positioning Systems, Inertial Navigation, and Integration*". John Wiley & Sons, Inc., Hoboken, New Jersey, ISBN: 9780470041901, 2007

8. Manfred Wieser. "*Reference Trajectory - exact knowledge of your path*". Institute of the Geodesy at the TU Graz, working Group Navigation, https://www.tugraz.at/institute/ifg/research/navigation/reference-trajectory

9. GlobalPOS. "*JAVAD*", GlobalPOS Pty Ltd, https://globalpos.com.au/collections/javad

10. Novatel. "*A NovAtel Precise Positioning Product- Waypoint Software 8.90 User Manual*". 2008

11. Franz Blauensteiner. " *GPS/IMU Integration für die präzise Bestimmung von hoch kinematischen Flugtrajektorien*". Master's thesis, TU Wien, 2008

12. Eun-Hwan Shin. " *Accuracy Improvement of Low Cost INS/GPS for Land Application*". Master's thesis University of Calgary, Department of Geomatics Engineering, 2001

13. Qing Li. *"GNSS/IMU based Vehicle Positioning".* Ahorn conference 2021

DI Qing Li graduated his master's degree in Geodesy and Geoinformation at Vienna University of Technology in 2014. After this he worked in the private business for 5 next years. He starts his PHD program in 2019 at TU Vienna. His research focuses on the tightly coupled Kalman filter by fusing of the GNSS, IMU and Odometer sensors. **Contact: Department of Geodesy and Geoinformation TU Wien, Vienna, Austria, qing.li@tuwien.ac.at**

Prof. Robert Weber is associate professor at the Department of Geodesy and Geoinformation, Vienna University of Technology, Austria. He received his Phd in 1990 on regional gravity field modelling. He spent two years as research assistant at the University of Berne dealing with satellite navigation and orbit determination. His main fields of research are Global Navigation Satellite Systems, geodetic Reference Systems, active GNSS reference station networks and applications of GNSS for geodynamics and meteorology. He passed habilitation in 2000 on the derivation of nutation terms from GNSS measurements and was member of the 2003 awarded EU Descartes Prize team (new non-rigid Earth nutation model). **Contact: Department of Geodesy and Geoinformation TU Wien, Vienna, Austria, robert.weber@tuwien.ac.at**

Back to table of contents

Instructions for EJN Authors

Volume of articles: Up to 10 pages (A4 vertical)

- The script shall be provided in MS WORD (.doc / .docx - format)
  main headers : Times New Roman bold 20
  headers: normal 16
  text: normal 11

- No page numbering

- Text to be provided in single column with graphics, tables, photos, etc. embedded in the text
  Please note: In addition, graphics/tables/photos should be submitted separately

- References should be listed at the end of the article

- Footnotes should be kept to a minimum

- A brief biography of the author(s) should be added separately (not part of the volume of the article) (name, photo, academic title(s), position, company/institution, address, e-mail address)

- For reference purposes, please provide in addition the complete article in .pdf format including all graphics and photos in the intended correct position of the script

- Headlines of paragraphs facilitate the formation of the article in the journal

Thank you!

Back to table of contents